UCL Université catholique de Louvain

École polytechnique de Louvain (EPL)

epl

# Towards nanostructured bioactive surfaces to control cell behavior

Dissertation presented by
**Thomas GRÉGOIRE**

for obtaining the Master's degree in
**Biomedical engineering**

Supervisor(s)
**Sophie DEMOUSTIER, KarineGLINEL**

Reader(s)
**Claire CHATTAWAY, Etienne FERAIN ,**

Academic year 2016-2017

# Acknowledgements

First, I would like to thank PhD student Claire Chattaway. She truly helped and guided me in the research and writing of my master thesis and was always ready to answer my questions.
I would also like to thank Pr. Demoustier and Pr. Glinel who helped and advised me in my work through monthly meetings but also in the everyday work.

Secondly, I would like to thank all people from the laboratory and WinFab room who helped me either way with a special thank to Delphine Magnin, Colette Douchamps, Cécile D'Haese, PhD student Eleana Somville and André Crahay who provided me with interesting and useful advices for the future.

Finally, I want to thank all my relatives (friends, family, sport club) who supported me the last years in my studies and helped me go through it. I especially thank Emmanuel de Sauvage for his great support and the accommodations he offered me.

I could not end those acknowledgements without expressing my profound gratitude to Emilie Monnart who has been to my side for 6 years, supported me in the bad and good moments and gave me continuous encouragements.

# Abstract

Controlling cell fate on artificial surfaces is of great interest in fundamental research but also more concrete fields as tissue engineering or cancer research. Nowadays, features up to the nanoscale are designed directly on the surface to allow manipulation of cell behavior. An example could be the modification of surface topography by decorating the surface with nanopillars. Such structures are interesting since, for specific aspect-ratios, they do not affect cell viability and can influence cell behavior. Moreover, such structures can also give access to the cell cytosol meaning drug delivery of desired compounds directly inside the cell can be obtained. Since cytosol can be regarded as a reducing environment, redox responsive layers grafted on the nanopillars could be an option for drug delivery applications. Indeed, if a drug is anchored through disulfide bonds to the nanopillars, it could be released thanks to the glutathione/glutathione couple present in the cytosol. Moreover, disulfide bonds also show an excellent stability in extracellular medium meaning the sample could safely be exposed to the cell external environment without undesired drug release.

The purpose of this work is to develop a bifunctionalized nanostructured surface. First, a flat surface is decorated with nanopillars. The top of the nanopillars is then coated with a polythiolactone copolymer on which a test component is grafted. The remaining surface is finally functionalized with a bioadhesive layer to promote cell adhesion on the surface and nanopillar endocytosis. The exposition of the top of the nanopillars to the reducing environment of the cytosol would result in the drug release inside the cell.
In order to perform this bifunctionalization, a sacrificial layer is used. This layer would cover the whole surface except for the top of the nanopillars that can be functionalized with the polythiolactone copolymer. Dissolution of the sacrificial layer is then performed and the remaining surface is available for the second functionalization.

Promising results were obtained for the different steps yielding to bifunctionalization of gold surfaces. Indeed, gold nanopillars of desired heigh and diameter were obtained on gold surfaces. Afterwards, the functionalization and bifunctionalization processes were studied and characterized. Polythiolactone copolymer grafting on flat and nanostructured gold surfaces was demonstrated. The spin-coating and etching of the sacrificial layer to reveal only the top of the nanopillars was also assessed and bifunctionalization could consecutively be performed. Finally, redox responsiveness of the copolymer layer when exposed to a reducing environment was assessed.
Platinum was studied as an alternative to gold but was not retained because of the poor copolymer anchoring on the metal.

# Contents

# List of Figures

# List of abbreviations

**AFM** Atomic force microscope

**BF** Blocking factor

**Cat** Chloramine T

**CV** Cyclic voltammetry

**DDT** Dodecanethiol

**DTT** Dithiothreitol

**ECM** Extracellular matrix

**EIS** Electrochemical impedance spectroscopy

**ETA** Ethanolamine

**PAA** Poly(acrylic acid)

**PC** Polycarbonate

**PEG-SH** Sulfhydryl poly(ethylene glycol)

**PMMA** Poly(methylmethacrylate)

**RIE** Reactive ion etching

**SAMs** Self-assembled monolayers

**SEM** Scanning electron microscope

**TlaAm** N-thiolactone acrylamide)

# Chapter 1

# Introduction

Nowadays, artificial and natural biomaterials take a great importance in medicine and biology, yielding to new scientific disciplines including tissue engineering which goal is to design artificial biocompatible structures that would substitute damaged tissues and organs. Moreover, biomaterials with well-defined design are also important for basic scientific research because they allow to study the signals controlling cell adhesion, spreading, growth, differentiation, functioning or viability [1] [2] [3].

In complex organisms, structural integrity, mechanical properties of tissues and cell properties like adhesion, migration, growth, secretion, gene expression and apoptosis are related to the cellular extracellular matrix (ECM) [4]. The interactions between the cells and their environment have therefore to be considered when manipulating cells in "in vitro" conditions. The first experiments performed to investigate specific cells interactions with the surface were conducted in 1956 by coating flat glass substrates with rat tail collagen [5]. In the following years, more researches were performed using more specific materials like extracellular matrix components, attachment and adhesive proteins (such as collagen, laminin or fibronectin) but also synthetic polymers [6].

Anchoring process of cells is directed by integrins which are transmembrane proteins linking the extra- and intracellular environment. Indeed, integrins are not only important for attaching a cell to its surroundings; they are also responsible for activating intracellular signaling pathways that will communicate to the cell the type of the extracellular matrix that is bond and eventually promote cell growth, cell survival and cell proliferation. [7].

However, because of their 2-D nature, traditional flat surfaces, even when coated with biological materials, are often not offering enough satisfaction for promoting in vitro cell functions, such as migration or differentiation. In order to mimic better the in vivo conditions of cells, 3D cell culture was developed.

First steps of 3D culture were done in the early 1960s when a study showed the effect of microtopography on cell migration by demonstrating that cell migration was more important on ridges than on grooves [8]. Nowadays, a myriad of techniques is used to produce surfaces with various topographies at different scales. These techniques alter surface topography at micrometer and nanometer scales and allow formation of very different structures including nanowells, nanopillars[1], nanotubes or nanorods that affect cell fate. This was notably evidenced through a study comparing cell behavior onto nanopillars and nanowells [9]. Conclusions were

[1]Both terms nanowires and nanopillars refer to cylindrical shaped nanofeautres present on a substrate. However, nanowires refers to higher aspect-ratio features then the one used for nanopillars. Since this distinction is not a consensus in the scientific field, nanopillars will be used along this work

that, compared to flat samples, cells preferentially adhered to pillars while there was no significant difference in cell adhesion onto welled structures. It was also demonstrated that, for specific sizes and diameters, nanopillars could access the cytosol [10] (through a mechanism of endocytosis), yielding interesting perspectives for specific release of components inside the cell.

However, cell anchoring is not the only process defining cell fate. Indeed, in their natural environement, they are exposed to perpetual physical and chemical changes. Therefore, having surfaces showing a variation of their properties when exposed to a specific stimulus like pH, temperature or electrical stimuli) is of interest to stimulate cell behavior. Indeed, this can possibly allow to control cell differentiation since cells have to adapt toward those changes. Obtaining such surfaces is often performed by material surfaces with different layers which are mostly based on self-assembled monolayers or polymer films [11]. Such surfaces are of high interest for biosensors [12], protein purification [13] but also drug-delivery [14]. One interesting example is related to the coatings based on redox-responsive polymers whose properties are modified when exposed to reducing or oxidizing conditions [15].

## Master thesis context

This work is part of a research project aiming at developing nanostructured and stimuli-responsive surfaces which are able to deliver drug locally to control cell behavior. Surfaces delivering drug at the nanometer scale, under redox stimulation, are notably aimed in order to control cell processes like cell fate, proliferation or apoptosis.

Nanostructured surfaces decorated with nanopillars present a great interest to control the cell processes at the nanometer scale [16]. Among the techniques used to fabricate such surfaces, the hard templating method using polymer track-etched membranes has been extensively studied, notably in our lab. Briefly, pores are created in a membrane and those pores are filled by a metal using electrodeposition. The polymer membrane is then dissolved revealing the nanopillars. Such nanostructures can be subsequently chemically modified in order to obtain bioactive surfaces that can address a specific (bio)chemical signal to a biological entity such as stem cells.
The aim of my project is to produce such nanostructured metal surfaces with the chemistry of the top of the nanopillars differing from the chemistry of the remaining surface. The top of the nanopillars would be modified with a stimuli responsive layer sensitive to a reducing environment such as the cellular cytoplasm. By grafting a specific component on this layer through disulfide bonds, the result will be the release of the component directly into the cell. The responsive layer chosen to functionalize the top of the nanopillars is a polythiolactone copolymer. The use of a polythiolactone copolymer is motivated by the high sensitivity of thiol groups to oxidation and therefore the need of a protection mechanism before the grafting on the surface. To achieve the thiol groups protection, they are trapped inside thiolactone rings. When the thiol functions are needed, an unprotection process is performed making some of the thiol functions available for copolymer grafting on the top of the nanopillars. The other ones are involved in the drug grafting and release in respectively oxidizing and reducing environments.
To provide bioadhesive properties to nanostructured surfaces, the remaining surface excluding the top of the nanopillars will be modified with a biofunctional layer presenting specific RGD sequences which are involved in cell bondings. This layer would also promote endocytosis of the nanopillars by the cell to expose the redox responsive layer to the cell cytoplasm.

The fabrication of the metal nanopillars will be first studied. The influence of different parameters, such as the operating conditions of track-etching and electrodeposition, on the shape, the height and the diameter of the nanopillars will be investigated. Afterwards, the work will focus on the selective surface functionalization of the metal nanostructures. We will notably

focus our work on:

- the grafting of polythiolactone copolymer layers onto both platinum and gold flat surfaces;
- the grafting of polythiolactone copolymer layers onto nanostructured gold surfaces and the preparation of bifunctionalized surfaces for which the chemistry of the top of the nanopillars differs from the remaining surface;
- the characterization of the nanopatterned surfaces;
- the study of the immobilization then release of model compounds onto the redox responsive polythiolactone copolymer layer.

This Master thesis is organized in 5 chapters:

- The chapter 2 described in detail the general objective of the project;
- The chapter 3 provides an overview of the literature on the fabrication and the biological applications of nanostructured surfaces;
- The chapter 4 is dedicated to materials and methods;
- The chapter 5 describes and discusses the results obtained;
- Finally the chapter 6 exposes the conclusions of this work along with some perspectives for the future.

# Chapter 2

# Objectives and strategy

## 2.1 Objectives

This work aims at developing redox-responsive nanostructured metal surfaces for drug delivery. This section will explain the general purpose of the master thesis and the reasons that lead to the strategy chosen to reach our goal. Afterwards, a more detailed explanation of the different steps will be developed.

A great number of studies were conducted in the field of cell behaviour on chemically and physically modified surfaces and a general conclusion is: cell behavior control is a challenging process and is highly dependent on cell type and surface properties[1]. In this work, different challenges need to be overcome: control the cell behavior on the surface, have a cytosol access and perform a drug release inside the cell.
To control cell behavior on the surface, two main mechanisms need to be controlled: cell adhesion and proliferation on the surface and cell differentiation in case of stem cells. Controlling cell adhesion, proliferation and differentiation can be achieved by integrating biological molecules (for example ECM proteins or specific protein sequences like RGD) and nanoscaled features on the surface. Moreover, adding specific bioactive species in the direct environment can avoid cell apoptosis and can also induce cell differentiation.
Afterwards, there is a need to work on the cytosol access as well as specific component grafting on the surface and release inside the cell. It was shown that cell can adhere on nanopillars without apoptosis. Moreover the height and the diameter of the nanopillars can be optimized to penetrate the cell membrane in order to deliver a biocative substance into the cell [17]. Using such structures would solve the second issue, namely cytosol access, and would leave one last problem to solve: drug anchoring on the surface and release inside the cell.
Since the cytosol can be seen as a reducing environment, the development of a redox-responsive layer which is able to release a bioactive substance in reducing condition is particularly attractive to modify the nanostructured surfaces. A polythiolactone copolymer used as redox responsive layer has intensively been studied in the work of S. Belbekhouche et al. [15]. The polythiolactone copolymer contains multiple thiol functions included into thiolactone rings in order to protect those functions from oxidation. The grafting of the polythiolactone on the substrate is performed by first opening of the thiolactone cycles using an amine component, revealing the thiol groups. Some of them are then able to graft on the surface while the remaining one are used for the grafting of a specific component through disulfide bonds cleavable in reducing environments. If cytosol access is achieved, drug release inside the cell through a redox reaction can be possible, solving the last issue.

By combining all solutions on one sample, we aim at producing nanostructured surfaces

[1] Section 3.4 gives an overview of the main achievements in this field

promoting cell adhesion and nanopillar endocytosis which, combined with a stimuli-responsive layer, leads to controlled release of a bioactive substance directly into the cell. Hard templating technique using track-etched membrane and metal electrodeposition will be combined with surface chemistry to produce such surfaces. However, we have here to coat the surface with two different materials (polythiols and biomolecules that favour adhesion). The proposed solution is to perform a spatially defined surface bifunctionalization using a polymer mask as sacrificial layer. This mask aims to cover the nanopillars base and substrate surface, revealing only the top of the nanopillars. This allows to coat only the tops of the nanopillars with the polythiolactone. The polymer mask is then dissolved, revealing the remaining surface which can be coated with the bioadhesive biomolecules. By doing so, we would obtain surfaces that gather all wanted features:

- the top of the nanopillars, coated with polythiols, that would penetrate the cell and release a target component through redox reactions;
- the bottom of the nanopillars and the bottom surface covered with bioadhesive structures that would enhance cell adhesion and nanopillars penetration.

Figure 2.1 shows an overview of the strategy which can be divided in 7 steps:

- metal surface elaboration using hard templating technique;
- deposition of a polymer mask on the surface;
- consecutive etching to leave only the tops of the nanopillars uncovered;
- modification of the top of the nanopillars by the polythiolactone;
- polymer mask dissolution;
- grafting of a SAM functionalized with RGD on the remaining surface;
- grafting of the model component on the polythiolactone through cleavable disulfide links.

Cell culture is one of the considered purpose for our bifunctionalized samples. However, this step is not represented here since this was not performed in this work.
The following sections will now describe more precisely how each step is planned to be performed. The exact protocol is given in chapter 4 "Materials and methods".

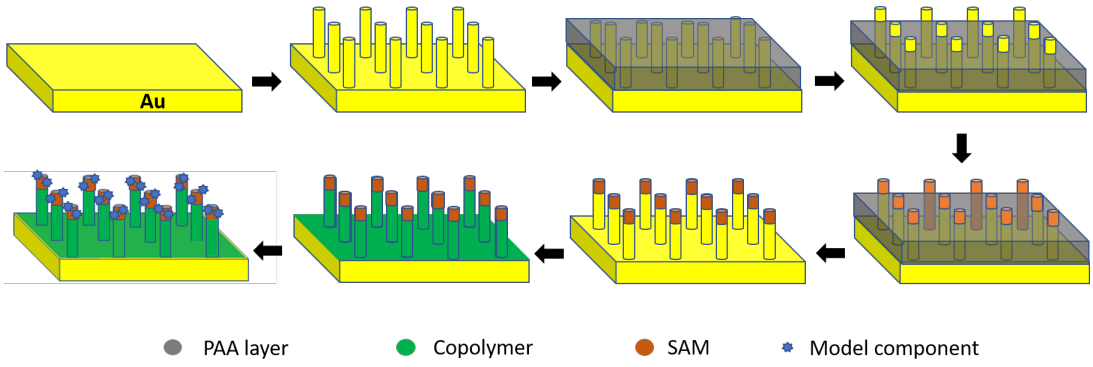


Figure 2.1: Main steps of the preparation of the bifunctionalized nanostructured surfaces

## 2.2 Detailed strategy

### 2.2.1 Nanopillars elaboration

Starting from flat gold surfaces, the goal is to electrodepose metal nanopillars with a height around 500 nm and a diameter around 100 nm. To this end, a hard templating strategy using

track-etched membranes is used. This process was intensively described in previous articles [18]. Basically, a polycarbonate (PC) layer is deposited on a gold surface using spin-coating. This coating is then irradiated by heavy ions to create linear tracks. Those tracks are subsequently revealed by a chemical etching to create pores that are consecutively filled with gold using electrodeposition. The PC layer is then dissolved to obtain to obtain a surface decorated with nanopillars. A schematic view of this process is displayed in figure 2.2, part 1.

### 2.2.2 Surface functionalization

The approach used to modify the metal surfaces is described in figure 2.2 (parts 2-3 ). It is a two step process:

1. a PAA layer is spin-coated on the surface and subsequently etched by plasma etching to reveal the top of the nanopillars;

2. because thiols are very sensitive to air oxidation, a strategy based on polythiols precursors is used. The top of the nanopillars is therefore grafted with a polythiolactone copolymer in presence of an amine derivative. This approach developed by Ghent University [19] is based on the use of thiolactone rings which contain thiols in a latent way. When thiol groups are needed, thiolactone copolymer containing thiolactone units are opened by a nucleophilic derivative such as an amine, releasing the thiol groups. The reaction is carried in presence of a gold surface on which a part of the released thiol groups is grafted while the remaining ones will be available for disulfide bonding with the drug;

3. the PAA layer is then removed to reveal the base of the nanopillars and the sample surface;

4. the base and bottom of the nanopillars nanopillars are subsequently grafted with a SAM of DDT. This SAM was chosen as a model to experiment the desired approach where bioadhesive factors are introduced on the surface to help cell attachment and proliferation and nanopillar endocytosis.

### 2.2.3 Grafting and release of a model thiolated compound onto the copolymer layer

The grafting of a model thiolated compound, namely Sulfhydryl poly(ethylene glycol)(PEG-SH), onto the free thiol groups of the copolymer layer was performed according to the protocol developed by Belbekhouche et al. [15]. Briefly, a thiolated compound is added onto the layer in oxidizing conditions to create cleavable disulfide bonds. The grafted substance can be subsequently released in reducing medium. This step is displayed in figure 2.2, step 4.

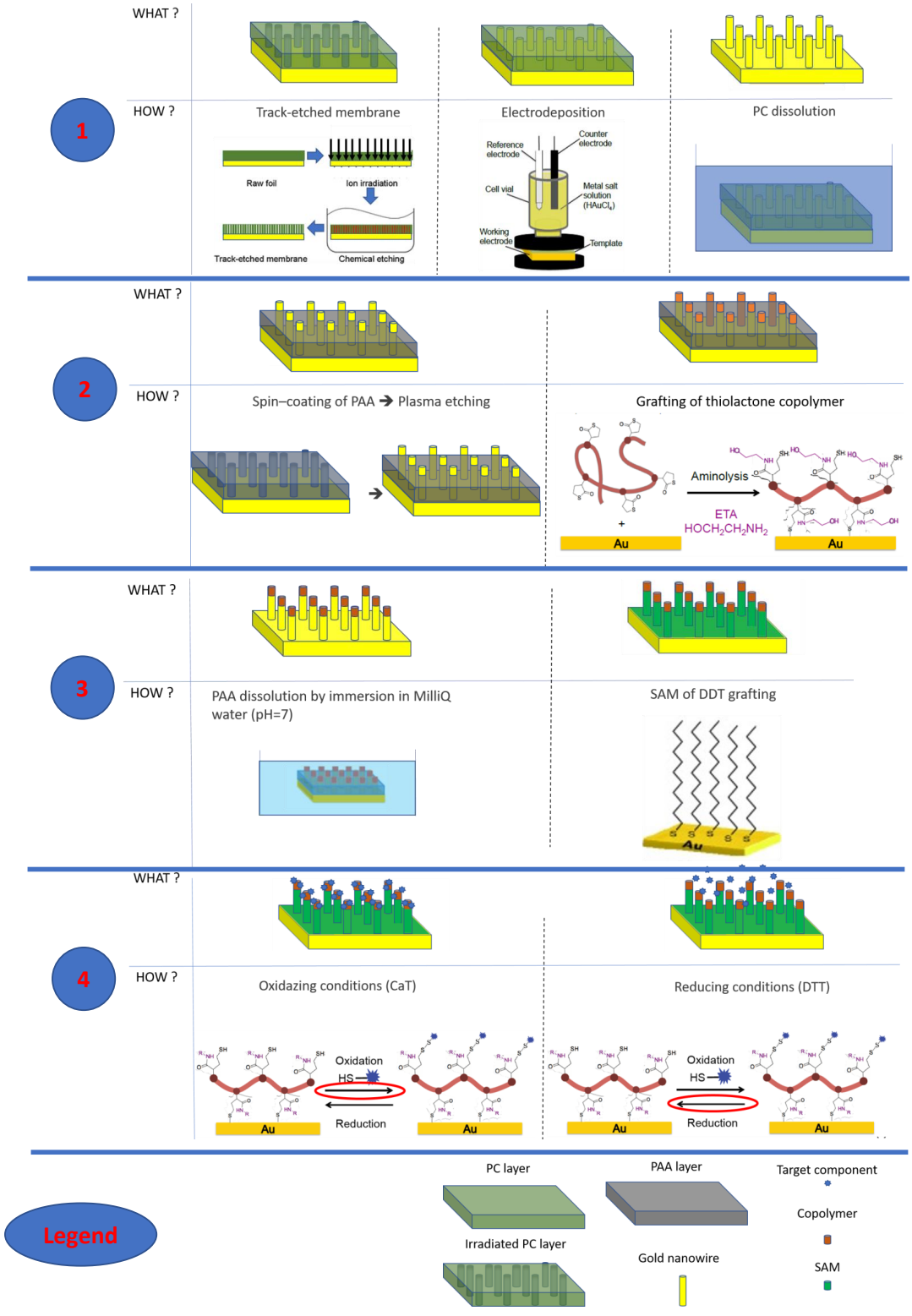


Figure 2.2: Detailed methodology used to prepare the bifunctionalized nanostructured gold surfaces: 1. Fabrication of gold surfaces decorated with nanopillars 2. Deposition of a polymer mask and selective exposure and functionalization of the top of nanopillars. 3. Polymer mask dissolution and grafting of a SAM on the open surface. 4. Selective grafting then release of a model thiolated compound on the copolymer coating.

# Chapter 3

# State of the art

Studies dealing with the fabrication of nanostructured and chemically modified surfaces designed for cell culture are legion. Indeed, since the considered dimensions are often smaller than the critical dimensions where classical physics apply, new and possible interesting features can be observed. This section gives an overview of what has been achieved in the fabrication and the application of nanostructured surfaces to control cell behavior. To this end, this chapter is organized into four sections: the elaboration of surfaces decorated with nanopillars, the description of the deposition and the processing of sacrificial or mask layers used to pattern a surface, the modification of metal surfaces by SAMs or polymer layers and finally the interactions of mammalian cells with patterned surfaces.

## 3.1 Elaboration of nanostructured surfaces

This section will describes in detail the template-assisted technique used to elaborate surfaces decorated with nanopillars. However, vapor-liquid-solid (VLS) is introduced since it is another widely used technique for nanopillars growth [20].

VLS is a chemical vapor deposition method[1] driven in the presence of a catalyst that accelerate the growth rate and allows creation of elementary or composite nanopillars [21]. This techniques offers the possibility to grow nanopillars directly attached to the substrates but requires special catalysts (e.g. transition metals like Fe, Ni or Co or noble metals like gold are often used) that highly dictate the shape and the distribution of the nanopillars onto the surface. In addition, there is an issue of potential incorporation of catalyst into nanopillars affecting their mechanical and chemical properties [22].

### 3.1.1 Template-assisted synthesis of nanopillars

The most commonly used and commercially available templates are anodized alumina membranes (AAM) and track-etched polycarbonate (PC) membranes [20].
The creation of pores in alumina membranes are made by anodic oxidation of aluminum sheet in sulfuric, oxalic or phosphoric acid solutions [23] [24]. A great advantage of this approach lies in the fact that pores can be arranged in a regular hexagonal array and densities as high as $10^{11}$ pores/$cm^2$ can be achieved with a pore diameter ranging from 10 nm to 100 $\mu$m [25] [26].

Template-assisted technique with PC membranes is commonly using a solution containing the species to be deposited such as metals, oxides, polymers or nanosized particles. The solution

[1]Process where one or more volatile precursors are transported via the vapor phase to a reaction chamber where they decompose on the surface.

hten fills a defined pattern printed on the PC membrane [20]. This process is less expensive than VLS and readily scalable to mass production. Moreover, the diameter, density and length of nanopillars are easily controlled independently and low contamination of nanopillars by other chemical products is observed. However, template-assisted synthesis suffers from the difficulties to find appropriate templates with pore channels of desired diameter, length and surface chemistry. In addition, the complete removal of the template is a critical step which can compromise the growth of the nanopillars [20]. Pores into PC membranes are obtained using mainly two different irradiation techniques: fission fragment tracking and accelerator tracking methods. The first technique is based on the use of fragments resulting from the fission of heavy nuclei. Since the emitted fragments have an isotropic angle distribution, a collimator is used to direct the beam onto the membrane [27]. The second approach is the use of an ion beam (which is frequently $Ar^{9+}$ accelerated at 220MeV [18]) created using an accelerator. This beam, composed of heavily ionized particles, interacts with the membrane and creates track changes along its trajectory in the material. If one compares both techniques, some advantages can be observed for the second irradiation technique compared to the first one [27]:

- there is no radioactive contamination;
- all tracks show the same etching properties due to identical bombarding particles identity;
- the energy of particles is higher so that thicker membranes can be tracked;
- track arrays with a higher density are easily produced (e.g. $\geq 10^9\ cm^{-2}$);
- the easy control of the direction of the beam allows to produce arrays of parallel pores.

For these reasons, the second technique has supplanted the first one despite its higher price and lower particle flow stability with time (i.e. meaning irradiation flow is more easily controlled when originating from fission fragment) [27]. When the irradiation step is completed, damaged tracks are turned into pores by treating the membrane with a temperature regulated chemical bath. The shape and diameter of the pores are directly influenced by the immersion time into the bath. This also means that pore density and diameter are nearly independent parameters and can therefore be varied in a wide range: pores diameter can vary between 10 nm up to 200 nm while pore density can lie between $10^5$ to $10^{10}\ cm^{-2}$ [27]. For PC layers, those baths are often hydrogen peroxide, caustic soda or acetic acid aqueous solutions [18]. An example of PC membrane irradiated then chemically treated is given in figure 3.1. It is important to note that some side steps allowing a better control of the nanofeatures are possible between irradiation and chemical etching to obtain nanopillars deposition in defined areas or enhanced shapes for the nanopillars (i.e. pores with a better cylindric shape, better chemical etching of the sensitized tracks).

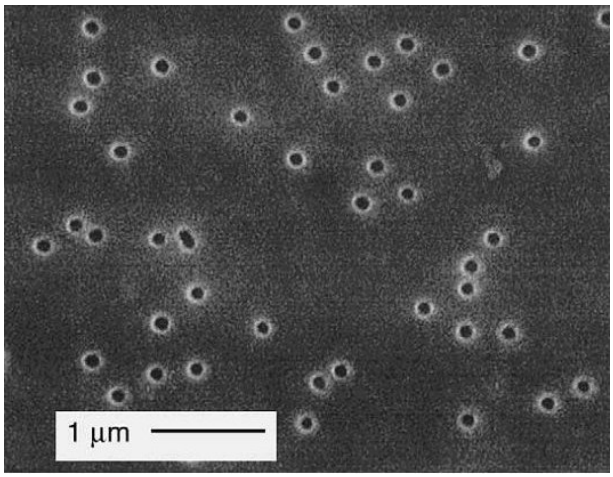


Figure 3.1: SEM image of an ion tracked etched PC membrane with pore diameter around 100 nm [28]

Apart from PC and aluminium membranes, other templates are also used such as nanochannel array in glass [29], mesoporous materials [30], porous silicon obtained by electrochemical etching of a silicon wafer [31] or bio-templates [32] [33]. It should also be noted that template-assisted synthesis is well-known for the growth of nanopillars but has been seen to attract an increasing attention for the synthesis of nanotubes, and in particular nanotube arrays [34]. One of the greatest advantages of template assisted synthesis for the growth of nanotubes arrays is the independent control of the length, diameter, and the wall thickness of the nanotubes. Indeed, while the length and diameter of the resultant nanotubes are dependent on the templates used for the synthesis, the wall thickness their wall thickness is readily controlled by the growth time [22].

### 3.1.2 Pore filling methods

When membranes are deposited on substrates and pores have been created into it, various techniques can be used to obtain nanopillars. They can be divided into three main categories [22]:

1. Electrochemical deposition (or electrodeposition) which is based on the deposition of charged species on a the conductive surface by the mean of an electrical current; only conductive species can be deposited by this method;

2. Electrophoretic deposition which uses oriented motion of charged particles in an electrical field to grow nanopillars; conductive and non-conductive materials can be deposited by this technique;

3. Template filling which consists in filling the pore by using a liquid precursor or mixture of reactives directly inside the pores.

Template filling is the most straightforward and versatile method to prepare nanopillar or nanorod arrays. Pore filling is achieved by different ways among which:

- Chemical polymerization for which a membrane deposited on a solid substrate is immersed in a mixture of monomer and initiator; the polymerization process occuring into the pores leads to the formation of polymer nanopillars [18].

- Electroless deposition which is performed using a reducing agent that is added to an electrolyte (i.e. solution containing the species to be deposited) and causes the species deposition; this approach is developed to prepare nanopillars used for sensor and separator applications [35].

The drawback of the template filling approach is the difficulty to ensure complete filling of the pores [22].
Because each technique uses different chemical and physical principles and is not suitable for a large range of materials, one shall choose the most adapted based on the requested nanostructure (e.g. nanopillars, nanorods or nanotubes). Focus is now given on electrodeposition.

**Electrochemical deposition**

If no template is present onto the surface, the electrochemical depostion will result in the whole coverage of the deposition surface by the coating specie. In industry, the electrochemical depostion is a widely used process for making metallic coating and it is known as electroplating [36]. However, in presence of a template, directed electrodeposition occurs in specific locations (i.e. pores in our case). A wide variety of conductive materials can be decorated by nanopillars according to this approach such as metals [37] [38], semiconductors [39], conductive polymers [40] [41] or oxides [42]. Alloys and composite materials could also be used for the coating [43]. However, we will focus on metal deposition since this is the material deposited in this work.
The typical assembly for an electrodeposition process is the following:

- an electrolyte, which is a solution containing the metal to be deposited. The composition of the solution can be varied and have a direct influence on the coating composition and properties (e.g. corrosion resistance, hardness, mechanical strength, ductility, ...) [44];
- a cathode, which is often the metal surface on which the deposition is performed;
- an anode, which can either be
  - a sacrificial anode which is dissolved during the electrodeposition process and therefore provides a continuous supply of the metal to be deposited
  - a permanent anode which closes the electrical circuit and does not provide a continuous supply of metal. In this case, the electrolyte should contain enough ionised metal required for the deposition process since none is created during the process like in the approach based on the use of a sacrificial anode.

The principle of the electrodeposition is based on oxidation/reduction reactions of the metal ions present into the electrolyte solution. Two reactions are considered:

$$M^{n+} + ne^- \rightarrow M$$

and

$$M \rightarrow M^{n+} + ne^-$$

There are mainly three types of metal deposition processes using an electrolytic cell [44]:

- Direct current electrodeposition for which a power source provides continuous current that flows through both electrodes and electrolyte, yielding to metal deposition;
- Pulse plating deposition for which a pulse current that can either be unipolar (on-off) or bipolar (current reversal) is applied in the electrochemical cell. By using the bipolar pulse, metal deposition occurs in the cathodic pulse period, with a limited amount of metal being redissolved in the anodic period. This repeated deposition and partial redissolution improves the morphology and the physical properties of the deposited feature [43];
- Laser-induced metal deposition which consists in applying a focused laser beam to accelerate the metal deposition rate that can be increased up to 1000 times by this process [43].

## 3.2 Polymer masks used as sacrificial layers

A sacrifial layer is defined as a layer of material deposited for mechanical separtion and isolation and that can be easily removed after a given physical or chemical treatment of the surface. [45]. It is mainly used in surface micromachining processes which designate a technique for microfeatures formation. An example of process is shown in figure 3.2. It illustrates a silicon substrate as a mechanical support and on which polysilicon nanofeatures are processed. The remaining layers that stay after the sacrificial layer dissolution are regarded as structural layers forming the desired micro-components [45].

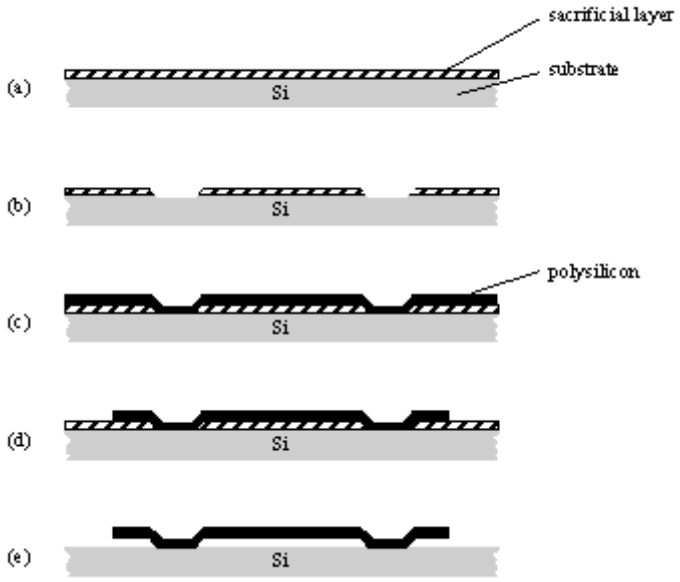


Figure 3.2: Basic surface micromachining process. (a) Sacrificial layer deposition. (b) Patterning of the sacrificial layer. (c) Deposition of the microstructure layer. (d) Patterning of the desired structure. (e) Stripping of the sacrificial layer reveals final structure [46]

### 3.2.1 Sacrificial layers composition and properties

In micromachining, inorganic materials like silica ($SiO_2$) are often used as sacrificial layers and can be dissolved using aqueous hydrofluoric acid (HF) or Reactive Ion Etching (RIE) [47]. HF is a well-known etcher that also etches a lot of other materials like metal oxides and organic polymers. However, problems occur with HF due to its poor selectivity (i.e. it tends to etch a broad range of materials and can therefore damage the mechanical support or micro-component) and its toxicity. This leads to an exclusion of a range of substrates (used as mechanical support) that are sensitive to HF.
Organic polymers (poly(imide), PMMA, PC, PAA and photoresist) are other type of materials used like sacrificial layer or material mask to protect the surface during a mechanical or chemical treatment. Depending on the polymer nature, different techniques are used to etch the polymer mask or layer: RIE, solvent dissolution, thermal degradation, ... . We will focus here on water-soluble sacrificial layers/polymer masks. Such sacrificial layers present some advantages: they can be deposited conveniently by spin-coating; the acqueous solvent can be removed at a low temperature (95–150°C) and the resulting layer can be dissolved in water which means that no corrosive reagents or organic solvents are required. PAA and dextran are very good examples of polymers used to prepare such sacrificial or mask layer because of their good solubility in water and insolubility in organic solvents [48].

### 3.2.2 Deposition techniques

Since spin-coating is the only technique that allow to deposit in a controlled fashion a water-soluble polymer layer on a substrate, we will focus on this technique. Spin-coating is based on the deposition of a thin poylmer film dissolved in a solution on a surface. If applicable, spin-coating is by far the most used technique for layer deposition. This is due to the many advantages it offers [49]:

- it is usually performed at room temperature;
- it requires considerably less equipment and is potentially less expensive;
- it can be used to coat large surfaces;
- small and well-controlled thickness are obtained.

A schematic example of a spin-coating process is given in figure 3.3. It consists in 4 main steps:

1. The material solution to be coated is deposited onto the sample center;
2. The sample undergoes a rotation at a defined speed. This will contribute to spread the polymer solution onto the surface while ejecting the excess of material due to centrifugal forces that induce a radially outward flow;
3. The rotation of the substrate is kept constant for a defined time to allow film homogenization;
4. Then the obtained film is annealed for a given time to remove the trace of solvent and to stabilize the film.

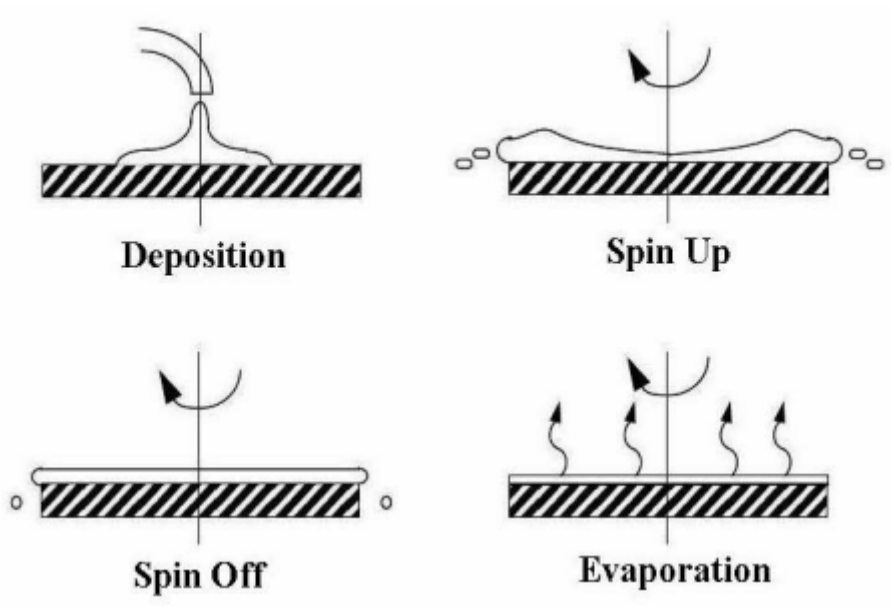


Figure 3.3: The four steps of spin-coating process. 1. Deposition of a polymer solution onto the substrate 2. Rotation of the sample leading to the spreading of the polymer solution and ejection of the solvent. 3. Film homogenization at a constant rotation 4. Solvent evaporation and film stabilization by annealing at high temperature [49]

The main parameters affecting the thickness of the spin-coated film are the rotational speed and the viscosity of the polymer solution which depends on the nature and the macromolecular

characteristics of the polymer as well as the nature of the solvent. For instance, the deposition of a PAA layer by spin-coating is influenced by the PAA concentration and the rotation speed used during the process as illustrated in figure 3.4.

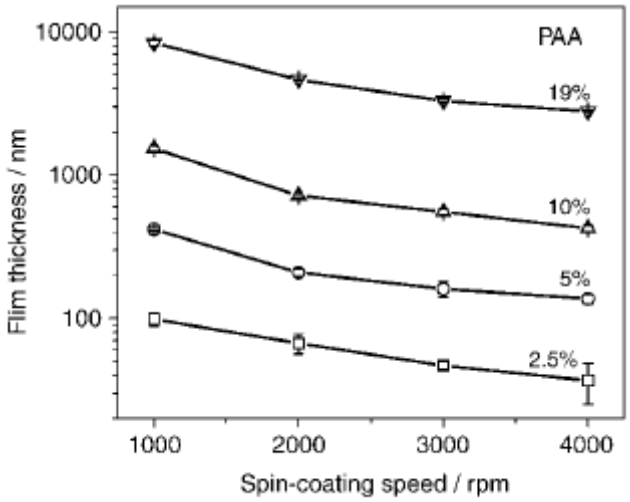


Figure 3.4: Thickness of PAA films deposited by spin-coating as a function of the spin-coating speed and the polymer concentration; the molar mass of PAA is 50 kDa. Error bars indicate the standard deviation with n=3 [48].

### 3.2.3 Etching techniques

The purpose of this step is to remove partially or fully the deposited material. Two types of etching can be distinguished: dry and wet etching. Whatever the type of etching considered, some properties characterize both etching processes [50]:

- etching rate i.e. amount of material removed per unit of time;
- etching uniformity which is related to the homogeneity of etching;
- selectivity of the etching of the desired material only.

#### Dry etching

Dry etching refers to etching performed by plasma or etching gases and is mainly an anisotropic process. In case of plasma etching, the principle is based on the creation of a plasma phase which is a partially ionized gas composed of electrons, ions and neutral species. The plasma is a neutral gas and has the same numbers of electrons and cations. An illustrative example of a plasma etching equipment is shown in figure 3.5.

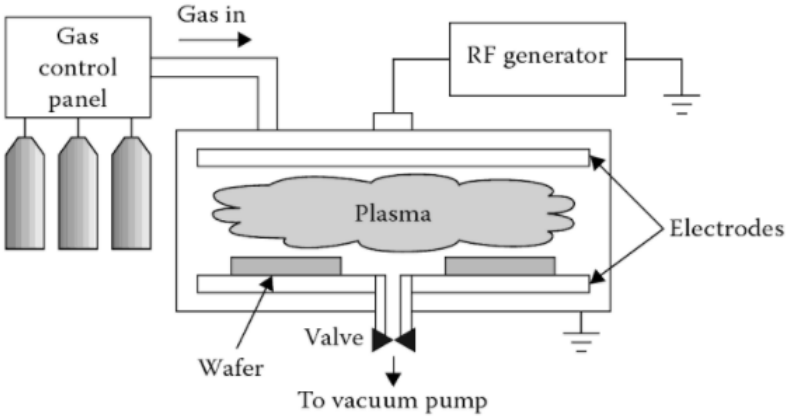


Figure 3.5: Schematic view of a plasma etcher machine [51]

To obtain a plasma, the starting point is the selection of a relatively inert gas or gas mixture. This gas or gas mixture is then pumped into the gas chamber where plasma is created by submitting the gas to a low pressure and either a direct current (DC) or a high-frequency voltage (in the range of radio frequencies) [52]. The different species composing the plasma phase will then lead to etching through three different mechanisms:

1. chemical etching is the result of chemical reactions that occur between the etched material and radicals present in the plasma. Tetrafluoromethane ($CH_4$), sulfur hexafluoride ($SF_6$), nitrogen trifluoride ($NF_3$), chlorine gas ($Cl_2$), or fluorine ($F_2$) are examples of gases used for chemical etching. [53]. Etching performed using this technique is more isotropic because reacting species can react in any direction and can therefore enter from beneath the masking material [54];

2. physical etching uses ions to knock out the atoms of the material, resulting in the evaporation of the material. No intended chemical reaction does occur in this kind of etching and it is quite an anisotropic etching since the ion flux is perpendicular to the surface;

3. Reactive Ion Etching (RIE) is a combination of the two types of etching mentioned above and is usually much faster than using only physical or chemical etching.

Based on the type of etching wanted, the samples are placed on the electrode connected to the ground or to the power supply.
If the sample is placed on the electrode connected to the ground (as displayed in figure 3.5), the electrical field around the sample is relatively weak and the kinetic energy of ions is not high yielding an etching principally occurring through chemical reactions.
If the sample is placed on the electrode connected to the power, the electrical field around the electrode is way more intense and ions with a high kinetic energy are obtained leading to a bombardment of the sample and therefore an important physical etching.
If the plasma phase contains reactive species and the sample is placed on the electrode connected to the power supply, both chemical and physical etching are observed leading to RIE [51].
Practically, a plasma is composed of a great diversity of species in the gas mixture which yield to uncontrolled side-reactions and makes it therefore hard to know exactly the type of reactions that occur in the chamber. After etching, the gas is simply pumped from the chamber.
Besides the gas or gas mixture composition and the location of the sample inside the chamber, other parameters do also influence the etching process such as the temperature which influences the etching rate and chemical reaction spontaneity, the power tension applied to the electrode, the pressure inside the chamber influencing the ion density and ion kinetic energy and the gas flow rate [55].

**Wet etching**

Wet etching is based on the use of an etching solution. In this process, the liquid etchant can easily access the whole surface meaning an isotropic etching is observed. The etching is the result of chemical reactions that consumes the targeted layer and produces side products. Such an etching can be represented by three main steps [56]:

1. The targeted layer is set into contact with the liquid etchant
2. The reaction between the liquid and the material occurs, resulting in the material dissolution
3. The diffusion of the byproducts into the solution.

When compared to dry etching techniques, this technique is usually cheaper and does not provoke possible toxic gas evaporation. On the other hand, it requires dangerous solvents and the wettability of the etched layer is not always ideal. Table 3.6 gives a comparison between dry and chemical etching.

| Parameter | Dry Etching | Wet Etching |
|---|---|---|
| Directionality | Good for most materials | Good only for single crystal materials |
| Automation | Good | Poor |
| Environmental impact | Low | High |
| Mask film adhesion | Not as critical | Very critical |
| Selectivity | Poor | Very good |
| Process compatible materials | Only certain materials | Nearly all materials |
| Scalability of process | Difficult | Easy |
| Cleanliness | Conditionally clean | Good to very good |
| Critical dimension control | Very good (<0.1 µm) | Poor |
| Equipment cost | Expensive | Relatively inexpensive |
| Typical etch rate | Slow (~0.1 µm/min) to fast (~6.0 µm/min) | Fast (~1.0 µm/min and above) |
| Operational parameters | Many | Few |
| Etch rate control | Good for slow etch | Difficult |

Figure 3.6: Comparison of Wet and Dry Etching techniques [51]

## 3.3 Surface modification

Modification of the materials surface is performed to alter the surface properties at different levels like biocompatibility [57] [58], wettability [57] [59], resistance to corrosion [60] or surface chemistry where a particular chemical functional is introduced at the sample surface [61] [62] [63]. It is also possible to perform surface modification to get switchable properties than can be tuned by an external stimulus. Such surfaces show the ability to provide spatially and temporally regulated responses triggered by a specific stimulus among which pH, light, temperature, electrical potential or redox environment [64] [65] [66]. Whatever the type of modification, their applications are wide and concern very different fields like microfluidic devices [67], biomolecule detection and separation [68] or drug delivery [69]. There are many different ways to modify the surface of a substrate and the chosen method usually not only depends on the desired properties of the interface. For example, if a hydrophobic surface is desired on a hydrophilic metal, there are methods available to add this hydrophobic layer. However, one method may require a complicated, time-consuming procedure but results in a highly stable layer while another may provide an easier process to depose a hydrophobic layer which is however less robust. The application should therefore be considered and balanced against these other factors when choosing a modification

method.
This section will first describes the modification of metallic surfaces by SAMs . Afterwards,the interest and the synthesis of polythiols used for stimuli responsive layers are detailed and finally, potential applications of such modified surfaces are discussed.

### 3.3.1 Metallic surface modification by SAMs

SAMs are organic assemblies formed by the absorption of small molecules from liquid or gas phases onto the surface sample and arranging naturally into crystalline or semicrystalline structures. The molecules used to form SAMs are composed of [70]:

- a head-group (or ligand) which has a specific and high affinity for a substrate;
- a hydrocarbonated tail (or chain) which determines the height of the SAMs layer. Tail–tail interactions, through van der Waals and hydrophobic forces, ensure an efficient packing of the monolayer, and its stability is increased with increasing chain length [71];
- a terminal functional group, which carries a desired chemical or physical function.

SAMs are grown on five main metals : silver, copper, nickel, palladium and platinium. Other composites do also support SAM growth like GaAs (Gallium arsenide) and InP (Indium phosphide). Many head groups can be used for SAMs grafting like carboxylate, phosphonate,isocynide,silane or thiol groups [72]. Figure 3.7 gives some examples of organic compouns with various compatible head groups.

| Surface | Substrate | Adsorbate(s) |
|---|---|---|
| **Metal** | Au | R-SH, R-S-S-R, R-S-R |
| | Ag | $R\text{-}NH_2$, R-NC, R-COOH |
| | Pt | R-NC, R-SH |
| | Pd | R-SH |
| | Cu | R-SH |
| | Hg | R-SH |
| **Semiconductor** | GaAs (III-V) | R-SH |
| | InP (III-V) | R-SH |
| | CdSe (II-VI) | R-SH |
| | ZnSe (II-VI) | R-SH |
| **Oxide** | $Al_2O_3$ | R-COOH |
| | $TiO_2$ | R-COOH, $R\text{-}PO_3H$ |
| | $YBa_2Cu_3O_7$ | $R\text{-}NH_2$ |
| | ITO* | R-COOH, R-SH, $R\text{-}SiX_3$ |
| | $SiO_2$ | $R\text{-}SiX_3$ |

Figure 3.7: List of head groups for specific substrates [73].

However, the most often studied head-group used for the linkage with a metal substrate is the thiol bond. Because each metal has a different structural surface chemistry, the SAM arrangement differs significantly from one metal to another one. However, all SAMs present a common structure (figure 3.8). It can be shown that two main parameters, namely $\alpha$ and $\beta$, characterize the different SAM arrangements onto the surface. Figure 3.9 shows typical angles for the anchoring of alkanethiols onto metallic surfaces [70]. We will focus now on thiol SAMs since those types were used in this work.

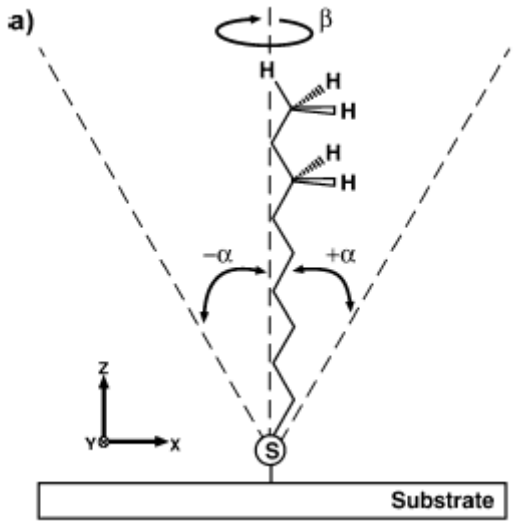


Figure 3.8: Schematic view of an all-trans conformer of a single, long-chain alkanethiolate adsorbed on a surface. The tilt angle ($\alpha$) is defined with respect to the surface normal direction. The twist angle ($\beta$) describes the rotation of the chain relative to the plane of the surface normal [70].

| Substrate | Cant Angle ($\lvert\alpha\rvert$) | Chain/Plane Rotation ($\beta$) | Characterization Method |
|---|---|---|---|
| Au(111) | 28° | 53° | RAIRS |
| Au(100) | 14° | 70° | RAIRS |
| Ag | 11-14° | 45° | RAIRS |
| | 13±2° | 44±6° | RAIRS |
| | 15° | 45° | Surface Raman Scattering |
| Cu | 12° | 45° | RAIRS |
| Pd | 16±2° | 45° | RAIRS |
| Pt | < 15° | n.a. | RAIRS |
| Hg | 0° | n.a. | X-ray scattering |
| | 0° | n.a. | Electrochemistry |
| GaAs(100) | 57±3° | 45±5° | RAIRS |
| InP(100) | 55±6° | n.a. | XPS |

Figure 3.9: Values of $\alpha$ and $\beta$ for n-alkanethiols adsorbed on a variety of materials. XPS = X-ray photoelectron spectrometry; RAIRS = Reflection Absorption Infra Red Spectroscopy [70].

Several factors affect the quality of the thiolate SAMs among which we can mention the crystallinity, the roughness and the cleanliness of the surface substrate, the nature of the adsorbate (the hydrocarbon chain length, the terminal group functionality, etc.), the temperature at which the thiol is adsorbed, the solvent used (e.g. ethanol, methanol, toluene, hexane, water, etc.), the immersion time and the concentration of adsorbate. Because of the above mentioned factors, the ideal representation of a perfect SAMs is far from reality [74].
A schematic view of an alkanethiols SAMs formed onto a gold surface is given in figure 3.10. The general formula of the thiol moelcules is given by $HS(CH_2)_nX$ with n, determining the tail length and X, the terminal function group. When an alkanethiol molecule comes into contact with the Au substrate at room temperature, the S-H bond breaks and the resulting thiolate forms chemical bonds with surface Au atoms [74].

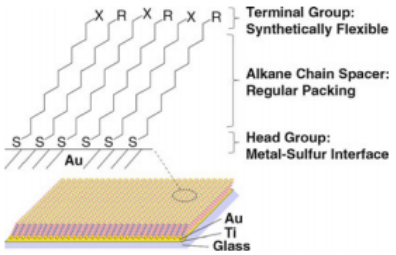


Figure 3.10: Structure of a SAM based on thiolated molecules and deposited onto a gold surface. SAMs are stabilized by the gold thiolate bond, which is nearly as strong as a covalent bond (around 200kJ/mol), and by the alkyl chain spacer via Van der Waals interactions. This provides a regular and tight packing. Terminal group are potentially accessible to immobilize ligands on the surface [75].

### SAMs on gold surfaces

Gold samples presents several advantages compared to other metals:

- gold is a well-known and widely studied substrate for thiol bonds formation;
- it is easily patterned by using a combination of lithographic tools;
- it is an inert metal: it does not oxidise with atmospheric O2; it does not oxidise at temperatures below its melting point; it does not react with most chemicals;
- strength of S-Au bonds is high, around 200kJ/mol, in the range of covalent bonds [70];
- gold is non-toxic for cells which is of primer interest in this work.

Moreover, the crystal configuration of deposited Au slightly influence the SAM formation and quality which means that SAMs growth on this metal is a quite easy and reproductible process [76]. Alkanethiols usually form SAMs with a higher degree of perfection on gold substrates [74]. In general, alkanethiol adsorption on gold is performed using thiol solutions with a concentration comprised between 10–1000 mM. Depending on the nature of the thiolated molecules, different solvents are used such as ethanol or methanol as well as different adsorption times (e.g. 2–12 h for long chain thiols, at least 24 h for short chain thiols). In biological applications, SAMs on gold samples are used in variated situations as biosensors, cell attachment or controlled protein adsorption [76]. An example of controlled protein adsorption is the engineering of a hydrophilic poly or tri(etheylene glycol) group into the SAM resulting in a monolayer which repels non-specific protein adsorption [77].

### SAMs on platinum surfaces

Platinum is more considered for microelectronics purpose, and particularly molecular electronics applications, because gold is essentially incompatible with Si CMOS technology due to its high diffusivity and electronic defects [78]. Platinum is far more subjected to oxidation when contacting atmospheric air and two approaches have therefore emerged to form thiolated SAMs onto Pt surfaces. The first approach attempts to avoid surface oxidation by minimizing exposure of samples to oxygen (deoxygenating solvents, handling samples in inert atmosphere). In the second approach, no explicit attempt is made to control the oxidation, and the deposition is carried out under more typical laboratory conditions (surface is cleaned by mechanical polishing or in a piranha solution) followed by alkanethiol deposition from an ethanolic solution. However, both approaches aim at avoiding the presence of the oxide layer on the surface. Indeed, it has been shown that on a freshly cleaned metallic platinum surface, the obtained SAMs are of high

quality [79]. On the opposite, if an oxide layer is present on the surface, a poor film quality is produced. Indeed, films were less ordered and more heterogeneous than the one obtained on non-oxidized platinum surfaces [79]. Therefore, although SAMs of high quality can be obtained on Pt surfaces, the experimental conditions for this are more drastic compared with the ones used to prepare SAMs onto gold surfaces. [79].

#### SAMs on other metals

Silver is also a well-known and studied option for thiol bonding but it oxydizes readily when contacting atmoshperic air(the same stands for copper) and is toxic for cells. Palladium seems to be the best alternative to gold for intented cell culture thanks to its low tendency to oxydize when contacting air and its biocompatibility [80].

### 3.3.2 Modification of gold surface by redox responsive layers based on polythiol

Polythiols are characterized by the presence of multiple thiol groups along the polymer chain. They are used in various situations likee drug delivery [15], optic fields [81] or microcapsules [82]. As shown in a previous work, the multiple thiol groups can be used for two different purposes. Some thiol groups are intented to be involved in the grafting onto the sample while the remaining groups would be available for selectivee bonding of target components using thiol chemistry [15]. The problem of such layers lies in the fact that polythiols are prone to oxidation in ambient environment so they have a very short shelf-life. Therefore such polymers are difficult to use to modify gold surface and to produce redox responsive layers. Moreover, the high thiol reactivity make it impossible to use most common polymerization techniques. Indeed, thiols iniate many side reactions with momoners and radicals [83]. In order to avoid both problems, precursors of polythiols containing protected thiol groups are synthetized. Further on, for the poylmerization process, one way is to include them into protective structures such as $S-alkyl-O-ethyl$ xanthate moiety groups [83] or thiolactone cycles [15]. The second option was studied and optimized by the group of F. du Prez at the Ghent University [19]. The thiol groups are incorporated in thiolactone cycles such as N-thiolactone acrylamide. Those monomers can then be copolymerized with acrylamide-based monomers (e.g. N-isopropyl or N,N-dimethylacrylamide). The polymerization is a controlled radical polymerization (CRP) like RAFT (Reversible addition−fragmentation chain transfer) or NMP (Nitroxide-Mediated Polymerization). This leads to copolymers with thiol groups that can subsequently be unprotected through aminolysis in presence of the sample, resulting in the sample decoration. Figure 3.11 shows the modification of the thiolactone-based copolymer.

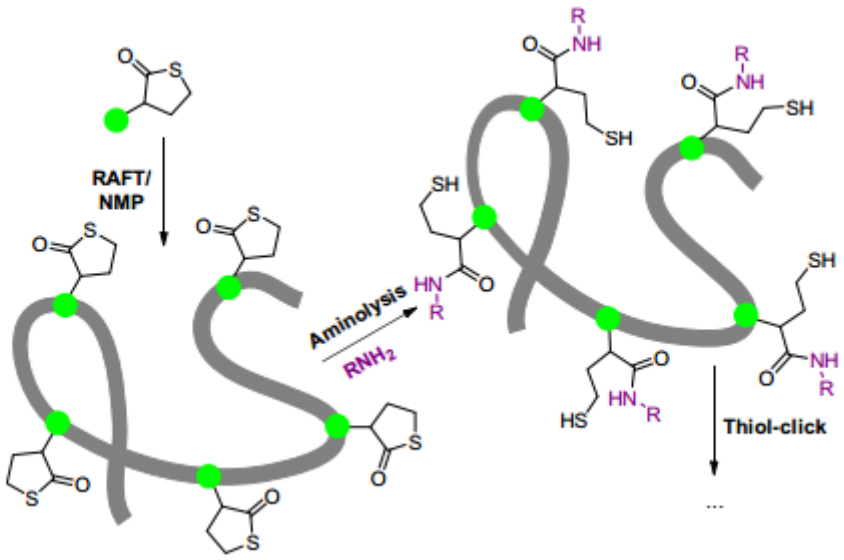


Figure 3.11: Schematic description of the double modification of pendant thiolactone moieties. After CRP (RAFT or NMP) of a stable vinylic thiolactone monomer, aminolysis of the linear poly(thiolactone) yields a linear polythiol, i.e. a reactive polymer scaffold for thiol modification [19]

The remaining thiol groups can be modified through click chemistry by formation of disulfide bonds. Such a bond is cleavable under reductive conditions and can be reformed under oxidative conditions which is of a great interest to form redox-responsive layers [15]. Given that thiols can be oxidized to sulfonates, the oxidative agent to form disulfide bonds should be carefully chosen.

## 3.4 Cell behavior on patterned surfaces

This section gives an overview of the cell behavior on patterned surfaces and focuses more precisely on cell penetration by nanopillars. Before jumping into these two points, lets consider cell fate in its natural environment.
Cells are submitted to many stimuli in a body from chemical to physical at the micro- or nanoscale. All those signals are spatio-temporally dependant and enable cells to be coordinate. More precisely, cells interact directly with the extracellular matrix (ECM). ECM can be defined as all the connective tissues and fibres that are not part of a cell but rather provide a support. ECM is also important in delimiting tissues from one another and regulating intercellular communication. The purpose of the following sections is to give an overview of what has been done and understood until now in cell behavior on artificial surfaces.

The interaction of cells with nanoscale topography has proven to be important in controlling cell function. Naturally occurring nanotopographic structures as well as synthetically nanofabricated topography can be used to influence cell morphology, alignment, adhesion, migration, proliferation, and cytoskeleton organization. The influence of surface topography on cell behavior was first evidenced by Harrison [84] and resulted in the concepts of contact guidance. This is defined by the response of cells to structures at the micron and sub-micron scale [85]. Mainly three basic nanotopographies are considered when studying cell behavior on nanostructured samples: nanogratings, nanoposts and nanopits (see figure 3.12).

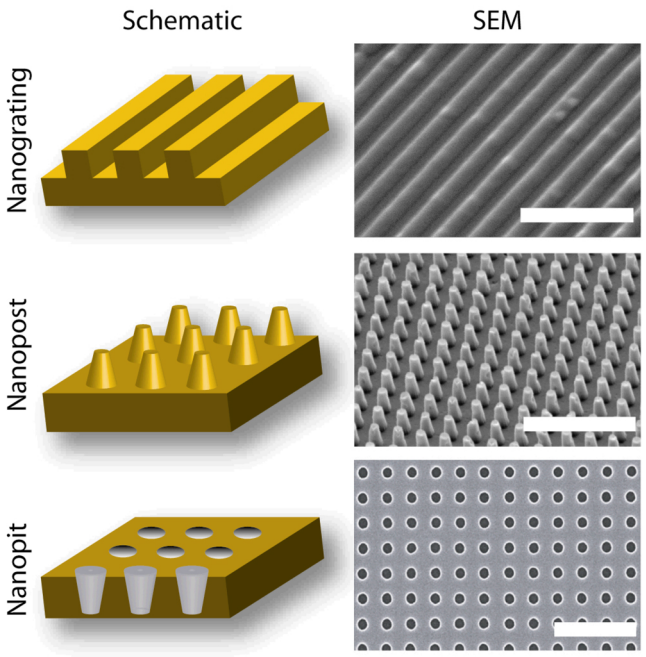


Figure 3.12: Schemes and SEM images of representative nanotopography geometries developped to investigate cell behavior. Three basic nanotopography geometries are displayed: nanograting (45° tilt, scale bar represents 5 $\mu$m), nanopost array (15° tilt, scale bar represents 5 $\mu$m) and nanopit array (0° tilt, scale bar represents 1 $\mu$m). Schemes not drawn to scale [85].

Adhesion of cells on the surface is a primer criterium of interest and is controlled by large protein scaffolds known as focal adhesion points. It has been shown that mimicking features of ECM could enhance attachment and cell adhesion [86]. In the same idea, anchoring specific proteins sequences to the surface (like RGD) involved in cell adhesion is also a solution to enhance cell adhesion. Indeed, RGD are involved in cell attachment and are found in numerous proteins and notably in integrins which are cell surface proteins linking the extra- and intracellular environment.
Cell morphology is one of the easiest and most observed feature on nanostructured surfaces. For example, on nanograting surfaces, some cell types tend to align and elongate parallel to the grating axis [87]. Other experiments where also conducted on nanoposts and nanopits were a reduction of spreading was demonstrated [85]. However, each cell type reacts differently on nanostructured surfaces and therefore, no general conclusion should be done.
Proliferation is also influenced by surface structuration. However, it is admitted that on nanogratings, cells exhibit reduced proliferation rates compared to cells cultured on planar substrates. For nanopits and nanoposts, studies showed opposite results that are hardly explained because mechanism are up to now little understood [85].
Finally, differentiation process is also influenced by surface topography. Indeed, it was for example shown that symmetry and order of nanopits significantly affected the expression of bone-specific ECM proteins [88].

### Cell behavior on nanopillars

During the last fifteen years, numerous research articles focused on biological applications of nanopillars. The possible applications are very broad and concern different fields like biomolecule detection and transport or mechanosensing [89]. Commonly, nanopillars are characterized by high-aspect ratios features cylindrically shaped. Studies showed that nanopillar density and array geometry, material nature and fabrication method affect cell viability, morphology and

behavior [89] [90].
Nanopillars negatively influences the cell spreading on the surface, leading to more rounder shapes than when grown on flat surfaces. Indeed, increasing nanopillars height and density lead to further decrease in cell spreading [91]. This is explained by the fact that cells are not able to reach the sample surface when density or height of nanopillars is too high resulting in the cells staying at the top of the nanopillars and therefore limited adhesion [90]. Usually, when density is higher then $30 * 10^6/cm^2$, cell adhesion is inhibited [92] while lower densities (i.e. $\leq 30 * 10^6/cm^2$) support or promote adhesion [91]. It should be noted that those values vary with the nature of materials used for the nanopillars growth.
Drug delivery applications is one of the great potentials of nanopillars. Shalek et *al* pioneered the silicon nanopillar assisted delivery of different bioactive substances such as proteins, DNA, siRNA and other biomolecules. They reported over 95% cells are penetrated by nanopillars [17]. To enhance cytosolic access, electroporation and lipid coating can be used. Electroporation uses an electrical field to acces the cytosol through the membrane while lipid coating aims to enhance the nanopillars endocytosis by the cells. Each technique possesses their advantages and drawbacks regarding feasibility, access duration or cell toxicity [90].

# Chapter 4

# Materials and methods

This section will detail the different methods and protocols followed during the master thesis. The first part will give the used chemical products for the experiments. The second part will highlight the experimental procedures and used equipments to perform them. Finally, the third part will give an overview of the different characterization techniques used to assess the results obtained through the experiments.

## 4.1 Purchased products and materials

### Solvents

Technical sulfuric acid ($H_2SO_4$) (95 %) was purchased from VWR chemicals. Hydrogen peroxide ($H_2O_2$) (30 wt%) was purchased from Chem-Lab. Absolute ethanol ($C_2H_5OH$) ($\geq$ 99%), methanol ($CH_3OH$) ($\geq$ 99.8%) and dichloromethane (DCM) ($\geq$ 99.5%) were purchased from AnalaR NORMAPURE ©VWR chemicals. Chloroform ($CHCl_3$) ($\geq$ 99.8%) was purchased from HiPerSolv CHROMANORM ©for HPLC VWR chemicals. Water ($H_2O$) was purified by Milli-Q ©water purification system with a resistivity of 18.2 $M\Omega$.cm at 25°C.

### Products

Ethanolamine (ETA) ($\geq$ 98%), 2-(N-morpholino)ethanesulfonic acid (MES), potassium hexacyanoferrate (II) trihydrate ($K_4Fe(CN)6.3H_2O$) ($\geq$ 98.5%), potassium hexacyanoferrate (III) ($K_3Fe(CN)_6$) ($\geq$ 99%), 4-(2-hydroxyethyl)-1-piperazineethanesulfonic acid (HEPES) ($\geq$ 99.5%), poly(acrylic acid) (PAA) solution ($Mw \sim 10000$, 35 $wt\%$ in $H_2O$), chloramine T (CaT) ($\geq$ 98%), dithiothreitol (DTT) ($\geq$ 98%), 1-Dodecanethiol ($C_{12}H_{26}S$) ($\geq$ 98%), gold (III) chloride trihydrate ($HAuCl_4.3H_2O$) ($\geq$ 99.9%), sodium hydroxide (NaOH) ($\geq$ 97%), TM-50 colloidal silica ($SiO_2$), Sulfhydryl polyethylene glycol (PEG-SH) (95%, $M_w = 2000g/mol$) were purchased from Sigma-Aldrich. Dow fax solution was purchased from it4ip. Potassium chloride (KCl) ($\geq$ 99.9%), anhydrous dipotassium phosphate ($K_2HPO_4$) ($\geq$ 99%) and potassium hydroxide (KOH) (ca. 85%) were purchased from Acros Organics.

The copolymer used in the work was synthetised by the group of Filip Du Prez from Ghent university according to a protocol described preivously [15]. Its chemical structure is shown in figure 4.1. After synthesis, the copolymer was purified by dialysis in water to remove residual monomers. The experimental value of thiolactone incorporated in the copolymer was measured by X-ray Photoelectron Spectroscopy (XPS) and elementary analysis. The molar mass and dispersity of the polymer was measured by size exclusion chromatography comparing the ratio of the percentage of nitrogen to sulphur and that of oxygen to sulphur. The copolymer has a number average molar mass (Mn) of 15kDa, a mass average molar mass (Mw) of 20.6kDa and a dispersity of 1.38.

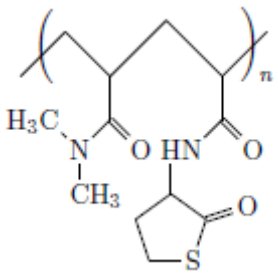


Figure 4.1: Chemical structure of P(DMA-co-TlaAm).

The copolymer is named P(DMA-co-TlaAm)-30% in the following. After aminolysis, the copolymer is named P(DMA-co-TlaAm)-30%-SH.

## 4.2 Experimental Section

This section is divided in three parts. First, the elaboration of gold nanopillars from a polycarbonate track-etched membrane is described[1]. Afterwards, the applied strategies for sacrificial layer deposition and partial etching are detailed. Finally, the methods for surface functionalization are given as well as the sacrificial layer dissolution.

### 4.2.1 Electrodeposition of nanopillars onto gold surfaces

The objective is to obtain electrodeposited nanopillars on a flat gold surface as shown in figure 4.2. We will go through each step from the silicon wafers (used as a mechanical support for the gold nanostructured surface and no represented on the figure) to the surface covered with gold nanopillars.

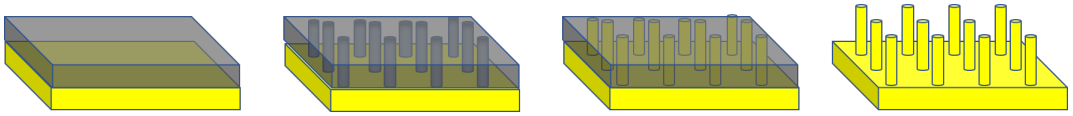

Figure 4.2: Successive steps from flat gold surface to nanostructured gold surface with nanopillars

#### Preparation of flat gold and platinum surfaces

Gold-coated surfaces are fabricated in a clean room (Winfab platform, UCL) environment by evaporating a 100 nm thick layer of gold on 10 cm diameter circular silicon wafers (100) precoated with a 5 nm thick layer of chromium to enhance adhesion. After gold deposition, surfaces are laser-cut into $1 \times 1\ cm^2$ squares.

#### Track-etching membrane technique

**Template elaboration and irradiation** Surfaces are first spincoated with a PC layer with a ca 1 $\mu m$ thickness using the following parameters: speed of 4500 rpm and a chloroform solution containing PC at a concentration of 95 g/l. Further on, in order to remove any trace of solvent, the PC film is annealed at 190°C for 4 h under vacuum. The irradiation is then performed by heavy ion bombardment ($Ar^{9+}$ at $220 MeV$) at the Cyclotron Research Center in Louvain-la-Neuve.

[1]It should be noted here that experiences were conducted on flat platinum surfaces to eventually switch from gold to platinum (reasons are explained in the "Results and Discussion" section). However, the results were not conclusive and work was continued on gold. If applicable, the experiments performed on platinum are similar to the ones conducted on gold.

As a result, the pore density in the membrane ranges from $10^8$ to $10^9$ $cm^2$. An UV treatment for 2 h is then performed to enhance pore size and shape.

**Chemical etching** To enlarge the pores and obtain the desired diameter(100 nm), samples are put 10 min in a 50:50 methanol:water solution containing 0.5 M sodium hydroxide and 0.1% (/v) Dowfax at 52°C. Surfaces are then rinsed during 2 min in a 50:50 methanol:water bath at 50°C. Solutions are changed every month to ensure good chemical etching. Samples are then dried under a nitrogen flux before submission to electrodeposition.

### Gold electrodeposition

Gold electrodeposition is performed by cyclic voltammetry on a potentiometer ChInstruments Chi660. The experimental set-up is shown in figure 4.3. Measurements are performed at room temperature in a one-compartment Teflon cell with a platinum counter electrode and an Ag/AgCl reference electrode. The sample placed between two rubbers is used as the working electrode. The electrochemical solution consists in: 6 mM $HAuCl_4$, 30 mM KCl and 30 mM $K_2HPO_4$. Solution is purged with nitrogen to avoid dissolved $O_2$ into the solution that could affect the gold deposition. The Teflon cell vial is then filled with the solution and electrodes are connected. The following operating parameters are used:

- Initial potential = 0.7 V
- High potential = 0.7 V
- Low potential = 0 V
- Initial scan polarity = positive
- Scan rate = 0.2 V/s
- Sweep segments = usually 10 or 15 (depends on the targeted nanopillars height)
- Sample interval = 0.001
- Quit time = 0
- Sensitivity = $10^{-4}$ A/V

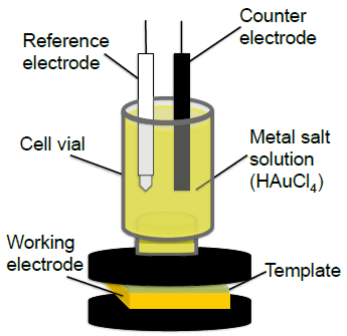


Figure 4.3: Experimental assembly of the electrochemical deposition. The three electrodes are linked to the Chi660 device

**Membrane dissolution**

In order to ensure complete and efficient dissolution, samples are:

- immersed at least 1 h into dichloromethane for 1 h and rinsed three times with the same solvent afterwards before being dried under a nitrogen flux;
- immersed into a 0.5 M NaOH solution for 1 h and rinsed three times with the same solvent afterwards before being dried under a nitrogen flux;
- placed into a plasma etcher to undergo a 10 min air(O2/N2) plasma treatment at 100 W using a K1050X RF Plasma Etcher/Asher/Cleaner from Emitech.

It should be noted that, to avoid wire breaking, PC membrane can be conserved on the surface until sample is needed.

### 4.2.2 Bifunctionalization of nanostructured surfaces

Once the surfaces are nanostructured, the next objective is the bifunctionalization of the nanopillars. The main steps followed are shown in figure 4.4.

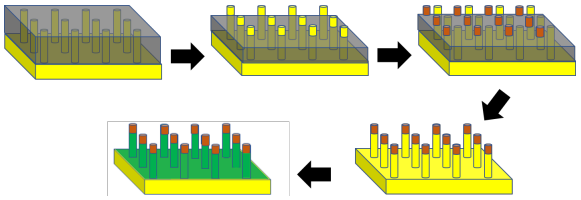

Figure 4.4: Main steps of the bifunctionalization

**PAA spin-coating**

PAA is used as a sacrificial layer and is spin-coated onto the surface. Spin-coating is performed both on nanostructured gold surfaces and silicon wafers. Silicon wafers are used to determine through ellipsometry the film thickness and the etched quantities since ellipsometry measurements are not compatible with gold surfaces.

**PAA solution preparation** Two different concentrations of PAA are spin-coated: 5 and 10% (w/v). The purchased PAA solution has an initial concentration of 35% wt. Therefore, it needs to be diluted with water to adjust the concentration. To determine the right volume to add, the following calculations are performed and explanations are given below:

1. $V_i[ml] = \dfrac{M_i[g]}{1.14[\frac{g}{ml}]}$ which gives the initial volume of PAA collected
2. $V_f[ml] = \dfrac{M_i[g] * 0.35}{C_{desired}[g/ml]}$ which gives the final volume to be obtained
3. $V_{H_2O}[ml] = V_f[ml]$-$V_i[ml]$ which gives the volume of water to add to the initial solution to obtain the desired concentration

Since the purchased PAA solution is too viscous, a spatula instead of a pipette is needed to collect a small amount of the solution. The taken solution is then weighted ($M_i$) and divided by the solution density (1,14 $\frac{g}{ml}$). This yields the volume of solution collected through the spatula.

The final volume to reach is calculated by multiplying the PAA mass ($M_i$) and the initial PAA solution concentration (35% or 0.35) and divide it by the desired concentration ($C_desired$). The amount of water to add is simply the difference between the final and the initial volume ($V_f$-$V_i$). When the solution has been diluted to reach the right concentration, mixing is performed for 20 min using a magnetic barrel. Afterwards, pH needs to be adjusted from 2 to 6-7. Therefore, a basic solution of KOH 8.93M is added to the PAA solution and pH is measured with a pH indicator paper. The solution is then mixed again for 30 min before using a laminar flow to filter the solution. An Acrodisc ©syringe filter with a 0.2 $\mu m$ pore size is used. Solution is then transferred to a 1/ISO 3 clean room and should be replaced every 2 to 3 months.

**PAA spin-coating** PAA is spin-coated on two types of substrates: silicon and gold. Before spin-coating, surfaces need to be cleaned to obtain homogeneous films. Two different protocols are defined depending on the surface to be spin-coated:

**Gold surface**

1. Rinse the surface using MilliQ water and ethanol before drying under nitrogen stream (repeat 3 times)
2. Perform UV-ozone for 20 min
3. Rinse the surface with ethanol and dry it under a nitrogen stream

**Silicon surface**

1. Cut surfaces using a diamond tip into squares of $1x1\ cm^2$
2. Rinse with MilliQ water and methanol
3. Gently wipe the surface with a KimTech paper
4. Rinse with methanol and dry under a nitrogen stream
5. Perform UV-ozone for 15 min
6. Rinse with methanol and dry under a nitrogen stream

Surfaces were then spin-coated in a 1/ISO 3 cleanroom (namely Winfab in UCL which is the micro- and nanofabrication platform of UCL). The spin-coater model used is the WS-650MZ-23NPP/LITE apparatus from Laurell.
A volume of 40 $\mu l$ of the prepared PAA solution is deposited at the surface center. The spin-coating process is then launched with the following parameters:

- Speed: 1750 rpm
- Acceleration: 875 rpm/s
- Duration: 60 s

The reason spin-coating speed is set at 1750 rpm/s is because, when PAA is spin-coated on the surface, nanopillars are undergoing important forces that could result in the bending and eventually breaking of the nanopillars [93]. Indeed, two main forces are exerted on nanopillars: a centrifugal force due to the sample rotation and a force due to the PAA moving towards the sample borders. To avoid this, the speed should be not too high to lower the centrifugal force and the PAA speed that flows towards the borders.
After spin-coating, the surface is placed for 2 min onto a hot plate at 150°C to evaporate the solvent. The surface is then stored away from the atmosphere to avoid water absorption by the PAA layer.

#### Etching of PAA layer

The etching process is performed as well on silicon samples as gold surfaces but for different purposes. The PAA layer on the gold samples is used to be able to obtain a bifunctionalized surface (see figure 4.4). Silicon surfaces were used to measure the thickness before and after etching by ellipsometry.
The etching was performed with two different plasma equipments. The first one is a K1050X RF Plasma Etcher/Asher/Cleaner from Emitech and uses air($O2/N_2$) as gas. Etching principally occurred through chemical etching. It will now be referred as the air plasma. The second one is a Electrotech ET340 RIE tool and uses oxygen as gas. Etching occurred both through chemical and physical etching. It will now be referred as the oxygen RIE. Since different powers were tried on both equipments (i.e. 100W on the K1050X and 1,2 and 3W on the ET340) to determine the best conditions for the PAA etching, the conditions used for etching (power,duration,plasma type) will be clarified when the results of PAA etching are presented in the Results and Discussion chapter.

### 4.2.3 Functionalization of gold surfaces

In this section, the anchoring of the copolymer, the SAM formation of dodecanethiol (DDT), the PAA dissolution and the anchoring and release of the test component are separately described. This choice was motivated by the fact that surface bifunctionalization was not directly performed. Indeed, prior to this, several tests were performed on flat gold surfaces to assess separately the success of the different approaches. Yet, the steps are presented in the right order to obtain bifunctionalized surfaces.

#### Copolymer grafting

The anchoring is induced by the opening of the thiolactone cycles through aminylosis (using ETA and ethylenediamine). To open the cycles, two different aqueous solutions are prepared:

1. Solution 1: The first solution contains 5 ml of chloroform and 3 mg of P(DMA-co-TlaAm)-30% prepared in a glass vial and is then mixed for 20 min using a magnetic stirrer.

2. Solution 2: The second solution contains 450 $\mu l$ of chloroform and 50 $\mu l$ of ETA to dilute ETA 10 times and is prepared in a glass vial.

Once solution 1 has been mixed, 10 $\mu l$ (2 molar equivalents) of solution 2 is added to it. After 30 s, the magnetic stirrer is removed and the cleaned gold sample is placed into the solution. At this point, the surface is left for 2 h into the solution to allow the anchoring of the copolymer on the surface. Figure 4.5 shows a schematic view of the reaction occurring. ETA acts as a nucleophile and opens the thiolactone cycles freeing the thiols which either attach on the surface or are available for disulfide bonding.

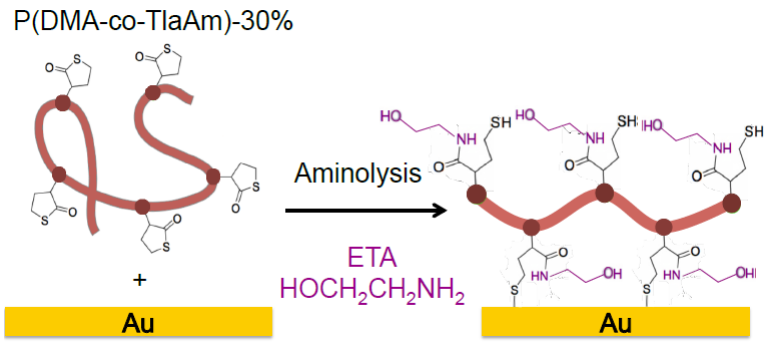


Figure 4.5: Immobilization process of the copolymer P(DMA-co-TlaAm)-30% onto the surface through aminolysis using ETA [93]

.

After the 2 h, surface is removed from the glass vial and gently rinsed with chloroform, ethanol, MilliQ water, ethanol and finally dried under a soft nitrogen stream. The whole functionalization approach is inspired from the work done by Sabrina Belbekhouche [15].

### PAA dissolution

When PAA layer is on the sample (i.e. in the bifunctionalization process), dissolution is performed since it is used as a sacrificial layer. The surface is immersed 3h in a MilliQ water solution at pH=7 for 3 h. This pH is reached by adding tiny amounts of KOH solution and measure it using a pH meter. The surface is then rinsed with MilliQ water and ethanol before being dried under a soft nitrogen stream.

### Formation of the SAM

The SAM chosen as model molecule is a DDT layer. The solution used for the SAM grafting, prepared into a glass vial, is a 20 mM DDT ethanol solution. The sample is immersed into it for 16 h. Afterwards, surface is rinsed with ethanol and then dried under a soft nitrogen stream.

### Anchoring and release of the test component

Finally, the last step is the anchoring and release of the test component PEG-SH on the copolymer.
The grafting occurs on the copolymer through disulfide bonds in an oxidative environment by using Chloramine-T (CAT) (chemical structure is given in figure 4.6). The choice of this component is motivated because of the high selectivity of CAT for disulfide bond formation [94]. Grafting and releasing of PEG-SH was characterized by Electrochemical impedance spectroscopy (EIS): the grafting and releasing of PEG-SH was thus performed in the electrochemical cell (see figure 4.3).

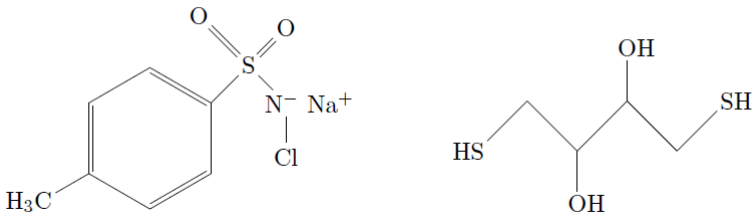


Figure 4.6: Chemical structure of Chloramine T (left) and dithiothreitol (right)

For grafting, three different solutions were prepared:

- Solution 1 (MES solution) is a 10 mM solution of MES buffered by MilliQ water (pH6)
- Solution 2 is a 1.5 mM solution of PEG-SH buffered by MES (10 mM, pH6)
- Solution 3 is a 2 mM solution of CaT buffered by MES (10 mM pH6)

In a typical grafting/releasing experiment, 100 $\mu l$ solution of PEG-SH is placed on the surface and 1 ml of CaT solution is added. The assembly is then placed on a rotating plate for 2 min. The solution is emptied, the cell vial is rinsed three times and EIS measurements (see section 4.3.1) are carried out.
The disulfide bond breaking is performed in an reductive environment using a 2 mM solution of DDT buffered by HEPES (10 mM, pH 7.2). DDT states for dithiotreitol which chemical structure is given in figure 4.6.
The cell, after being rinsed three times with MilliQ water, is filled with the reductive solution and is placed again on the rotating plate for 10 min. The cell is then emptied again, rinsed three times with water and EIS is performed again to see if PEG-SH has been released.

#### Bifunctionalization assessment

To assess the bifunctionalization of the surface, silica nanoparticles were used. The top of the nanopillars was functionalized with the copolymer in presence of ethylenediamine and the background with DDT. The negatively charged nanoparticles should only interact with the positively charged copolymer (on the top of the pillars) and not with the hydrophobic substrate. Copolymer initial concentration was decreased to 0.1 mg/ml and 10 molar equivalents of ethylenediamine were used instead of 2. Basically, the same functionalization protocol was used leading to bifunctionalized nanopillars with their top positively charged. Afterwards, the surface was immersed in a silica nanoparticle solution prepared as follows: 200 $\mu l$ of colloidal silica were added to 20 ml of MilliQ water. The solution was consecutively sonicated for 30 min then filtered using an Acrodisc(c) syringe filter (0.2 $\mu m$) and sonicated 10 min. The solution was stirred with a magnetic stirrer for 10 min before being used.
The sample was immersed vertically in the nanoparticle solution during 5 min then rinsed in three differents baths of MilliQ water: 15x1 s in the first, 7x3 s in the second and 3x30 s in the third. The sample was then immediately analysed by using a Scanning Electron Microscope (SEM), namely a Jeol 7600F device.

## 4.3 Characterization techniques

This section aims to give an overview of the equipments and detail how the measurements work. The equipments and their use in this work are described in the following:

- electrochemical techniques: electrodeposition of nanopillars ; functionalization assessment of sample by the copolymer and/or DDT ; grafting and release of PEG-SH ;
- ellipsometer: PAA layer thickness before and after etching;
- atomic Force Microscope (AFM): surface topography before PAA spin-coating, after PAA spin-coating and after PAA etching;
- scanning Electron Microscope (SEM): nanopillars characterization after electrodeposition and PAA spin-coating ; bifunctionalization assessment using silica nanoparticles.

### 4.3.1 Electrochemical techniques [95]

The conductivity of platinum and gold make them amenable for performing electrochemical measurements. Electrochemical techniques acquire data at an electrode-solution interface and are used as a link between electricity and chemistry. In other words, the measurements make the link between electrical quantities (such as current, potential or charge) and chemical reactions occurring in the solution. At least two electrodes are needed for the simplest electrochemical measurements but most of the time, three are used: a working (or indicator) electrode, which is often the studied sample, a reference electrode, which potential is known and remains constant, and a counter electrode that completes the electrical circuit. Based on such configuration, basically two different measurements can be obtained:

- measure the potential while controlling the current (potentiometric measurements)
- measure the current while controlling the potential (amperometric measurements)

For amperometric measurements in a quiescent solution, three types of potential variations are commonly used: linear, pulsed or cyclic potential. The resulting current induced between the working and the counter electrode is then measured. By applying a potential that is higher (lower) than the standard-state potential of a targeted analyte, oxidation (reduction) of the analyte occurs at the working electrode and a faradaic current flows through the cell. This faradaic current can be of two types: "anodic current" in case of analyte oxidation (negative sign) or "cathodic current" in case of reduction (positive sign). Therefore, the rate of the redox reaction occurring at the working electrode can be determined by mean of the measured current. This current is affected by mainly two parameters: the mass transport of analytes into the solution (i.e. rate and means at which analytes reach electrode surfaces) and the efficiency of electron transfer between the electrode and electroactive species, which depends on the kind of reaction, the electrode type and the temperature.
Three different mass transport can be distinguished:

- Diffusion
- Migration
- Convection

Diffusion occurs when a concentration gradient is created between the electrode surface and the bulk due to reduction or oxidation of the analyte at the surface of the electrode. This phenomenon is essential to always observe a current flowing in the cell.
Migration is the result of attraction or repulsion between a charged electrode and charged species in the electrochemical solution. This kind of mass transport is unavoidable but can be neglected in the measurements by adding high concentration of electrochemically inert species (that will not be oxidized or reduced). This was done in the master thesis by adding high quantities of KCl into the electrochemical solution.

Convection forces are not present since no stirring occurs into the electrochemical cell.
It can be therefore assumed that the only mass transport measured in the solution is diffusion. The current flowing in the cell therefore follows:

$$i = \frac{nFAD(C_{bulk} - C_{x=0})}{\delta}$$

where n= number of electrons in the redox reaction, F = Faraday constant, A= the electrode area, D = diffusion coefficient of analyte, $C_{bulk}$ and $C_{x=0}$ = concentrations in bulk solution and at the electrode surface,$\delta$ = thickness of the diffusion layer.
There also exists a so-called non-faraidic current resulting from the charging of the electrode. Indeed, if, for example, the working electrode is positively charged, cations and anions in the solution will respectively move away or towards the surface electrode. This results in a low and temporary current that persists until the positive charge of the electrode is counterbalanced by the negative charge of the solution at the electrode surface. This leads to the existence of an electrical double layer at the electrode surface that influences and limits the measurements of controlled potential measurements.

### Cyclic voltammetry

In voltammetry, a time-dependant potential is applied on the electrochemical cell and the resulting current is measured. From this, a voltammogram showing current flow versus potential can be plotted. Depending on the type of mass transport occurring into the electrochemical solution, different voltammograms are obtained. Indeed, if convection is included in the mass transport phenomena, a limiting current will be reached because the diffusion layer ($\delta$) is constant (figure 4.7). However, if convection is not present, a peak is observed because the diffusion layer becomes thicker (figure 4.8).

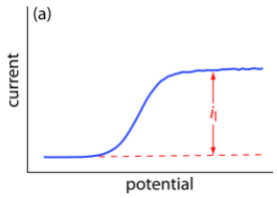


Figure 4.7: Current as a function of the applied potential when convection and diffusion defines mass transport phenomena [95].

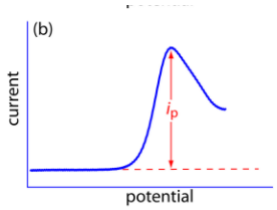


Figure 4.8: Current as a function of the applied potential when only diffusion define mass transport phenomena [95].

Cyclic voltammetry (CV) is a particular case of voltammetry where potential is swept in both potential directions (i.e. positive and negative values). Figure 4.9 shows the potential variation for one cycle. Of course, this cycle can be repeated several times.

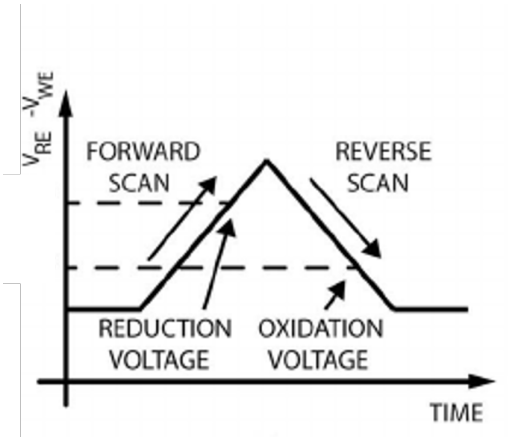


Figure 4.9: Cyclic potential applied between the reference and working electrode [96].

An example of typical voltammogram is given in figure 4.10. This plot was obtained on a gold surface and can be read as follows:

- point A: Potential is increased positively and a resulting current, due to the oxidation of the analyte (here $Fe(CN)_6^{4-}$ into $Fe(CN)_6^{3-}$), increases positively until a maximum value (B);
- at point B: The current drops because the diffusion layer becomes thicker. Indeed, the oxidation rate is higher than the diffusion rate resulting in an accumulation of oxidized analyte at the electrode interface and diffusion layer is therefore increased;
- at point C, potential is reversed and is decreasing towards negative values. Oxidative reactions still occur but the rate is lowered and current is therefore also decreased until 0 (Point D). A diffusion-controlled peak can be observed;
- current is now negatively charged indicating reduction of the analyte. Potential will be reversed again (point F) until point A where a new cycle begins. A diffusion-controlled peak is also observed here but this time due to the accumulation of reduced analyte at the electrode interface.

This kind of voltammogram is obtained when the rate of reaction is limited by mass-transport. However, cyclovoltammetric measurements in this work were performed on bare gold surfaces, surfaces covered with the copolymer or surfaces covered with the SAM, both acting as insulators. Therefore, the rate of reaction is limited by the transfer of electrons through the insulation layer and smaller currents are thus measured resulting in decreased curve area. This reduced area was used to quantify the quality of the covering of the surface by the SAM or the copolymer by computing the Blocking Factor (BF):

$$BF = \frac{A_{bare} - A_{covered}}{A_bare} * 100\% \tag{4.1}$$

with $A_{bare}$ and $A_{covered}$, the areas on the voltammogram curve for respectively bare and covered surface.

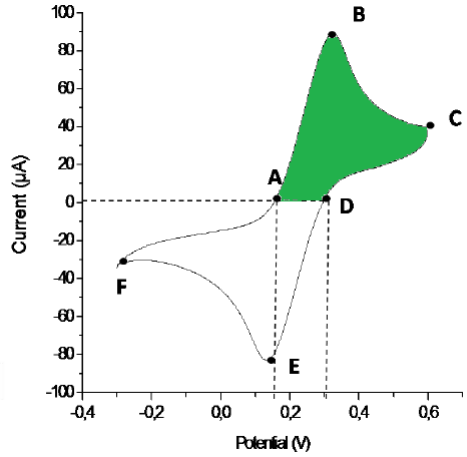


Figure 4.10: Typical voltammogram of cyclic voltammetric for a 1 mM solution of $Fe(CN)_64-$ / $Fe(CN)_63-$ and 0.1M of KCl, using bare gold surface as a working electrode, platinum as counter electrode ang Ag/AgCl as reference electrode. The green area represents the measured area for computing the Blocking Factor [97].

A ChInstruments Chi660B is used to perform the measurements and the experimental assembly is identical to the one used for the nanopillars formation. The electrochemical solution contains the $Fe^{2+}/Fe^{3+}$ couple and more precisely, 1 mM of $C_6FeK_4N_6.3H_2O$, 1 mM of $C_6FeK_3N_6$, 100 mM of KCl and 100 ml of MilliQ water as solvent. The solution is consecutively purged with nitrogen to evacuate oxygen from the solution in order to avoid oxygen reduction into hydrogen peroxide during the measurements that would create a small current and noise in the acquired data. The following parameters are set for the measurements:

- Initial potential = 0.2 V
- High potential = 0.6 V
- Low potential = -0.3 V
- Initial scan polarity = positive
- Scan rate = 0.1 V/s
- Sweep segments = 20
- Sample interval = 0.001
- Quit time = 0
- Sensitivity = $10^{-4}$ A/V

The kind of data acquired through those measurements are used to estimate the covering of the surface via BF. The seventh and eighth scan are systematically taken to measure this value. However, CV is not sensitive enough to distinguish the grafting and release of thiolated compounds. Consequently, another technique is used for this assessment, namely Electrochemical Impedance Spectroscopy.

### Electrical Impedance Spectroscopy (EIS)

The principles of EIS will first be described. We will then briefly introduce the electrical circuits that could possibly model the electrochemical cell and finally, we will show how, based on the

electrical circuits, one can interpret the data obtained with EIS.
The basic principle of EIS is the following: an AC voltage with varying frequencies is applied on an electrochemical cell and the variation of the impedance is observed. Impedance is defined as the whole complex resistance of an electrical circuit against the flow of an electric current. When the AC voltage is applied, only small excitations are used to stay in a linear system (i.e. keep a steady-state in the electrochemical cell). By this mean, the flow of current induced by the sinusoidal potential variation is also sinusoidal with the same frequency but a phase shift. Based on this, impedance can be defined using Ohms law (R=E/I) as:

$$Z(w) = \frac{E_t}{I_t} = \frac{E_0 sin(\omega t)}{I_0 sin(\omega t + \phi)} = {}^2Z_0(cos(\phi) + jsin(\phi)) \tag{4.2}$$

This equation shows that the impedance is defined through a real and imaginary part. If those two quantities are plotted, a so-called "Nyquist plot" is obtained. Another representation, called "Bode plot" can also be used to represent the impedance. In that case, variation of frequency or phase are displayed with respect to the change in frequency. Figure 4.11 shows the typical plots obtained.

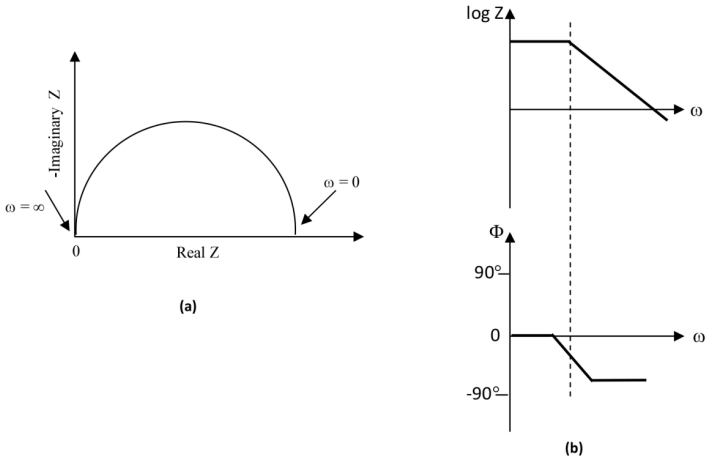


Figure 4.11: a) Nyquist plot showing real vs imaginary part of impedance. (b) Bode plots showing the variation of impedance (log Z) or phase angle ($\phi$) with respect to change in frequency [98].

Once those graphical representations have been obtained, they can be compared to theoretical plots given by electrical circuits that represent the electrochemical cell. Different circuits can be used to model the cell simply by adding specific components that would represent a specific phenomena (diffusion, resistance to charge transfer, ...).
The simplest electrical circuit used to represent an electrochemical cell is the Randle circuit (see figure 4.12). It includes the double layer capacitance ($C_{dl}$), the ohmic resistance of the solution ($R_s$) and the resistance to charge transfer ($R_{ct}$). The associated Nyquist plot is given in figure 4.13 and is always a semi-circle. Moreover, each component of the circuit can be identified on the Nyquist plot and the electrochemical cell properties can therefore be determined. Indeed, $R_s$ correspond to the left intersection of the semi-circle with the $real_i$ axis while $R_ct$ is given by the distance between the two intersections of the semi-circle.

[2]This equality is found through Euler relationship: $exp(j\phi) = cos(\phi) + jsin(\phi)$

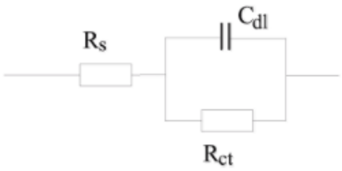


Figure 4.12: Simplified Randles Cell Schematic Diagram with $R_{ct}$ = charge transfer resistance, $R_s$ = solution resistance, $C_{dl}$ Double-layer capacitor [99].

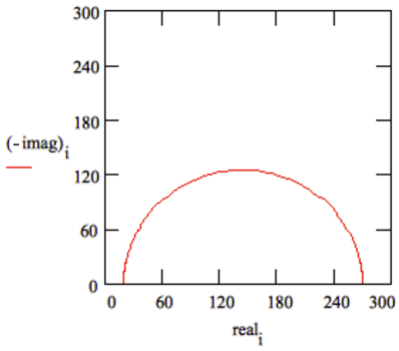


Figure 4.13: Nyquist plot based on the Randle circuit [99]

More complicated electrical circuits and associated Nyquist plots can be determined as adding a Warburg element to the Randle circuit to model the ion diffusion from the bulk solution to the electrode surface (see figure 4.14). The Nyquist plot is then influenced in consequence because of the change in impedance of the circuit (see figure 4.15).

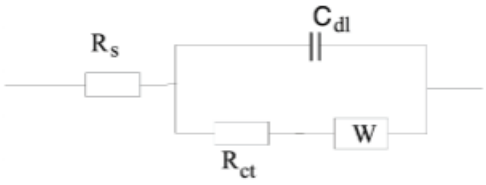


Figure 4.14: Randle circuit with added Warburg element to model the ion diffusion from the bulk solution to the electrode surface [99].

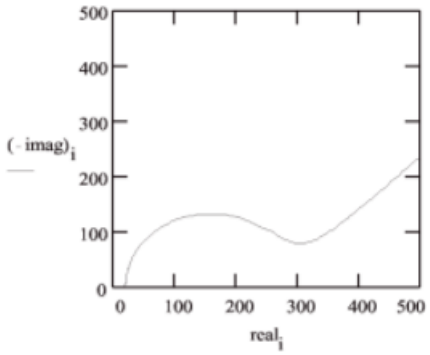


Figure 4.15: Nyquist plot based on the Randle circuit with Warburg element [99].

When EIS measurements are performed on covered gold samples with the copolymer, the Nyquist plot obtained is similar to the one in figure 4.13. This is because the copolymer can be modelled as a charge transfer resistance that thus significantly increases the intrinsic charge transfer resistance of the system yielding to a Nyquist plot dominated by this aspect with a semi-circle of high diameter. However, when EIS measurements on bare gold surface are done, Nyquist plots resemble to the one obtained in figure 4.15. This is because charge transfer resistance is low while mass transfer resistance is high and because principal mass transfer occurs through diffusion which means the Warburg element models well this phenomenon.
Measurements were performed using the same assembly and solution then the one used for CV. However, in order to let the system reach its equilibrium, it was left behind for 30 min after filling the Teflon cell vial. The measurements were performed using the following operating parameters:

- Initial potential = 0.2 V
- High frequency = 100 000 Hz
- Low frequency = 0.01 Hz
- Amplitude = 0.01

- Quiet time = 0
- Sensitivity = $10^{-4}$ A/V

### 4.3.2 Ellipsometry

Ellipsometry is an optical characterization method used to measure a broad range of properties of a material (optical constants, roughness, composition, thickness, ...). This technique offers, inter alia, a high resolution (up to the Angstrom), the possibility to work with single or multi-layered samples and a non-destructive way to collect the data. Figure 4.16 shows the main steps of ellipsometry measurements. We can see that the obtained measurements need to be fitted to models in order to extract the wanted information meaning the choose of the model is a critical step. The whole process is described more precisely below.

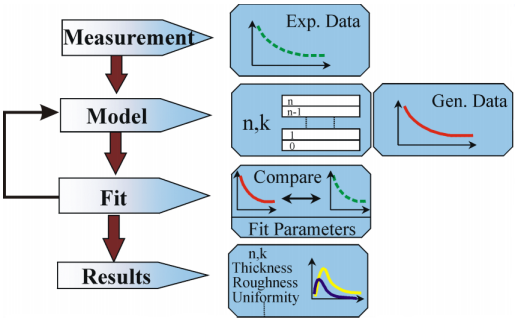


Figure 4.16: Main steps of ellipsometry measurements and data fitting [100].

The measurements are based on the change in polarity of a light beam after reflection on a surface. More precisely, an elliptically polarized light beam (polarization refers to the wave electric field behavior in space and time) is directed towards the sample and is then reflected or transmitted (see figure 4.17). This modifies the light polarization and these changes can be quantified by considering the ratio of the parallel ($r_p$) and perpendicular ($r_s$) components of the electromagnetic wave associated to the light beam before and after reflection using Fresnel equations.

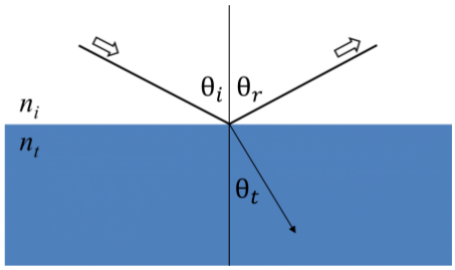


Figure 4.17: Light reflects and refracts according to Snell's law [101].

$$r_p = \frac{E_{rp}}{E_{ip}} = \frac{n_t cos(\Theta_i) - n_i cos(\Theta_t)}{n_t cos(\Theta_i) + n_i cos(\Theta_t)} r_s = \frac{E_{rs}}{E_{is}} = \frac{n_i cos(\Theta_i) - n_t cos(\Theta_t)}{n_i cos(\Theta_i) + n_t cos(\Theta_t)} \tag{4.3}$$

with $n_i$ = real index of refraction of the ambient, $n_t$ = real index of the refraction of the sample ; $\Theta_i$ = the angle of incidence ; $\Theta_t$ = the angle of transmission.
In ellipsometry, both phenomena (changes in polarization and phase before and after reflection) can be defined by two parameters: $\Phi$ and $\Delta$. $\Delta$ represents the phase difference before and after

reflection while $tan(\Phi)$ represents the amplitude ratio between $r_p$ and $r_s$ waves. Both are linked by the following equation:

$$\rho = \frac{r_p}{r_s} = tan(\Phi) * e^{i\Delta} \tag{4.4}$$

These are the two values measured by the ellipsometer. However, this does not give any indication on the layer's thickness. Therefore, one needs to fit the data to a model. The accuracy of the film-thickness will thus depend on the reliability of the used model. It is important to note that different ellipsometers exist among which spectroscopic and single wave-length ellipsometers. The first one is characterized by the use of a broad range of light sources (covering infrared, visible or ultraviolet spectral) but keeping the Angle Of Incidence (AOI) constant, yielding to many sets of $\Phi$ and $\Delta$. On the other hand, the second one employs a monochromatic light source but changes AOI, yielding to one set of $\Phi$ and $\Delta$ per measurement.
Ellipsometric measured were performed using two different spectroscopic ellipsometers. The first one is a Sentech SE 850 with broad ban light sources (190-900 nm), an AOI of 72° and using the SpectraRay Software. The second one is a single-wave ellipsometer (EP4 from Accurion). The model used for determining the PAA layer thickness was composed of the ambient air (refractive index set to 1) and three different layers:

- the silicon substrate: the optical properties are given by the database of the SpectraRay software;
- the $SiO_2$ layer: silicon samples are covered with a very thin layer (around 1.5 nm) of SiO2. The Cauchy equation is used to compute the refractive index (evolving with the wavelength):

  $$n(\lambda) = n_0 + \frac{n_1}{\lambda^2} \tag{4.5}$$

  with $n_0 = 1.452$ ; $n_1 = 36$ and $\lambda$ the wavelength;
- the PAA layer, whose thickness is to determine. Cauchy equation is used again to compute the refractive index but with different $n_0$ and $n_1$ (1.474 and 47 respectively). To compute the thickness, an estimation of the thickness needs to be introduced in order to allow the model to make the iteration in the appropriate thickness window.

### 4.3.3 Atomic Force Microscope

This technique was used to observe the bare surface when only nanopillars are present onto the surface as well as the nanopillars coverage after PAA spin-coating.
The equipment used is a Bruker Multimode Nanoscope V with a tilt compensated high aspect ratio AFM tip (type AR5T-NCHR-10, produced by Nanosensors) on the cantilever, which is designed to scan nanostructured surfaces.

### 4.3.4 Scanning Electron Microscopy

This technique was principally used to characterize the nanopillars electrodeposited onto the sample (shape, diameter, height, density). It was also used to observe if the silica nanoparticles adhered to the modified copolymer when we want to assess bifunctionalization (see section 4.2.3). The equipment used is a JEOL 7600F. Different acquisitions (type of electrons measured and detector position) are possible using semi-inlens secondary electrons detector, lateral secondary electron detector or backscattered electron detectors (classical and LABE). The images produced in this master thesis were acquired using only secondary electrons with a beam energy set at 15keV.

# Chapter 5

# Results and Discussions

This section will give an overview of the results obtained during the experiments conducted in the laboratory. Moreover, a discussion and a critical analysis will be done to explain and understand the obtained results. The order of presentation is the following:

- elaboration of gold nanopillars through electrodeposition using hard-templating technique;
- spin-coating and etching of the sacrificial layer;
- functionalization of flat platinum and gold samples by the thiolactone copolymer and grafting/release of the test-component;
- bifunctionalization of gold nanopillars.

## 5.1 Surface nanostructuration

The different stages followed to obtain samples decorated with nanopillars can be separated in two main steps. The first step is represented in figure 5.1 and concern the creation of linear damaged tracks in the PC membrane. First, a PC membrane is spin-coated on the sample. It is then irradiated using an ion beam in order to create linear damaged tracks. Finally, the damaged membrane is exposed to UV in order to enhance nanopillars shape. Afterwards, the pores creation and filling is performed as shown in figure 5.2. The pore revelation is done by immersing the sample in a chemical bath. This bath has an influence on the final diameter of the pores (the longer the sample stays, the larger the pores are). In order to increase the sample wetting, a Dowfax solution is added to the chemical bath. Those pores are finally filled by mean of electrodeposition and the PC layer is dissolved to reveal the nanostructured sample. In this section, two different operating conditions are studied:

- the influence of UV treatment on the nanopillars shape (see third step in figure 5.1);
- the effects of switching from an old Dowfax solution to a new one the nanopillars diameter and the random electrodeposition phenomenon (step 1 in figure 5.2).

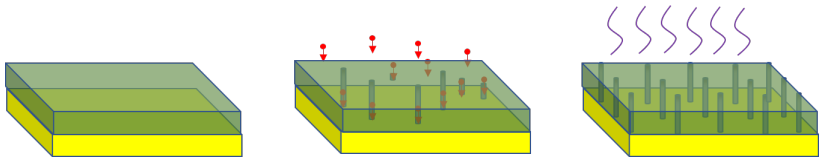

Figure 5.1: Successive steps of the PC membrane damaging. 1. Deposition of a PC membrane on the gold sample through spin-coating. 2. Membrane irradiation using a heavy ion beam. 3. UV treatment of the damaged membrane

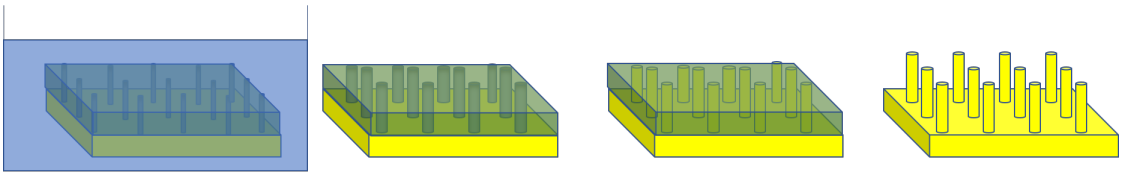

Figure 5.2: Successive steps for the pores revelation and consecutive electrodeposition. 1. The damaged PC membrane is immersed in a chemical bath to enlarge the pores. 2. Pores of desired diameter are obtained. 3. Electrodeposition of gold inside the pores. 4. Dissolution of the PC membrane revealing the surface decorated with nanopillars.

The samples presented here followed the same electrodeposition conditions (i.e. 10 sweep segments at a scan rate of 0.2 V/s between 0 and 0.7 V). To conclude this section, the typical distribution of nanopillars heights and diameters on the surface are given.

### 5.1.1 UV treatment of irradiated PC layer

We will first observe the critical impact of UV treatment before chemical etching. Figure 5.3 and 5.4 shows the comparison between two samples where UV treatment was performed or not on the PC layer after the heavy ion irradiation in the cyclotron. There is a clear presence of tooth-pick shaped nanopillars if no UV treatment is performed beforehand.

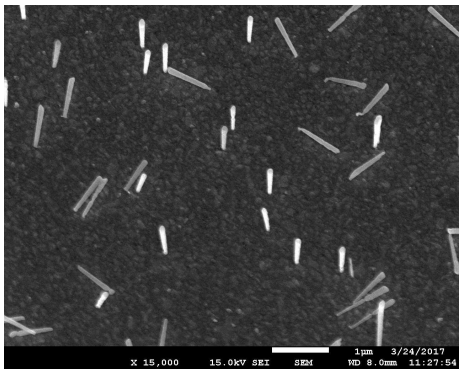


Figure 5.3: SEM image of a surface electrodeposited at a scan rate of 0.2 V/s, 10 scans and without prior UV treatment

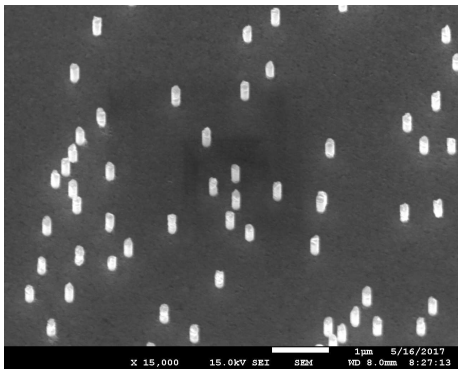


Figure 5.4: SEM image of a surface electrodeposited at a scan rate of 0.2 V/s, 10 scans and with prior UV treatment

Tooth-pick shaped nanopillars confirm the observations made in a previous article where it was shown that pore shape is not cylindrical but rather toothpick-shaped [102] [103] when no UV treatment is performed after PC irradiation.

### 5.1.2 Dowfax influence on nanopillar diameter and random electrodeposition

A fresh and old Dowfax solution were used in this master thesis and an increase in nanopillars diameter was observed using the new solution (138 +- 6 nm against 103 +- nm ). Moreover, a higher percentage of random electrodeposition was also observed as shown in figure 5.5 and 5.6.

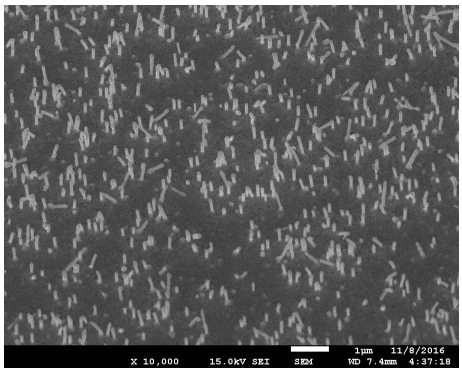


Figure 5.5: SEM image of a surface where chemical etching was performed in a bath containing the old Dowfax solution

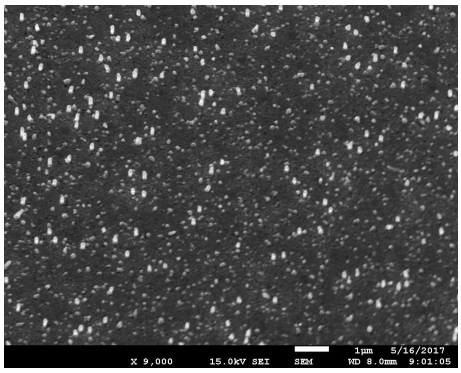


Figure 5.6: SEM image of a surface where chemical etching was performed in a bath containing the new Dowfax solution

Dowfax seems to have a great influence on the diameter of the nanopillars. Indeed, when taking identical operating conditions and only changing the Dowfax solution, a difference of nearly 40 nm is observed. This could be due to the better wetting efficiency of the new Dowfax resulting in a better diffusion of the etching solution inside the tracks created during the PC layer damaging by heavy ion beams.
Another observed phenomenon was the increase of random electrodeposition with the new Dowfax. Indeed, when comparing samples exposed to the new and old Dowfax, random electrodeposition increased from 22% (2 out of 9) for the old solution to 60% (9 out of 16) for the new solution. This phenomena is harder to explain but could be the consequence of a slight PC membrane detachment resulting from the immersion in the chemical bath.

### 5.1.3 Typical height and diameter distribution

If UV treatment is performed before immersion in the chemical bath and if the old Dowfax solution is used, the typical heights and diameters of nanopillars obtained are given in figures 5.7 and 5.8. Both height and diameter do not follow a Gaussian distribution. On average, heights are around 350 to 500 nm and diameters are ranging from 95 to 110 nm.

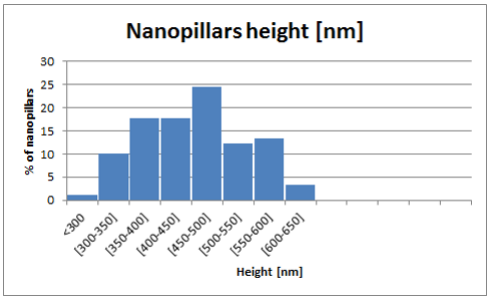


Figure 5.7: Average height of 90 nanopillars of a typical electrodeposited surface at a scan rate of 0.2 V/s and using 10 scans

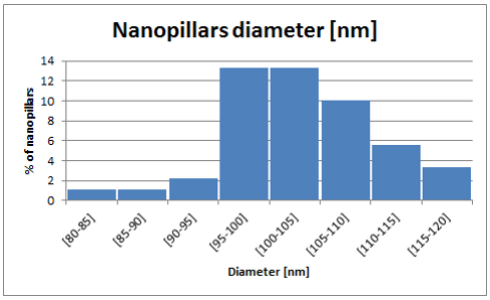


Figure 5.8: Average diameter of 45 nanopillars of a typical electrodeposited surface at a scan rate of 0.2 V/s and using 10 scans

Ten scan numbers allow to obtain nanopillars with a limited aspect-ratio, a desired feature so that the nanopillars would not break or bend easily. Indeed, as shown in a previous work [93], too important aspect ratios could lead to bending and breaking of nanopillars especially when submitted to spin-coating. Since our nanopillars will be subjected to spin-coating, a limited aspect-ratio was targeted. The reason why nanopillars are sensitive to this process can be explained using the stress formula obtained by using beam theory. Indeed, it can be shown

that stress is proportional to $h^2$, h being the nanowire height, and inversely proportional to the nanopillars radius ($1/r^3$, r being the nanowire radius) meaning that lower heights (and therefore lower aspect-ratios) will result in decreased stress in the nanopillars.

## 5.2 Sacrificial layer

A sacrificial layer was used in this work to obtain bifunctionalized nanostructured samples. Figure 5.9 shows the main steps of this strategy. First, the PAA layer is spin-coated on the surfaces. A plasma etching is then performed to uncover and clean the top of the nanopillars which are then functionalized with the thiolactone copolymer. The PAA layer is then dissolved to reveal the remaining surface which is now available for the second functionalization.

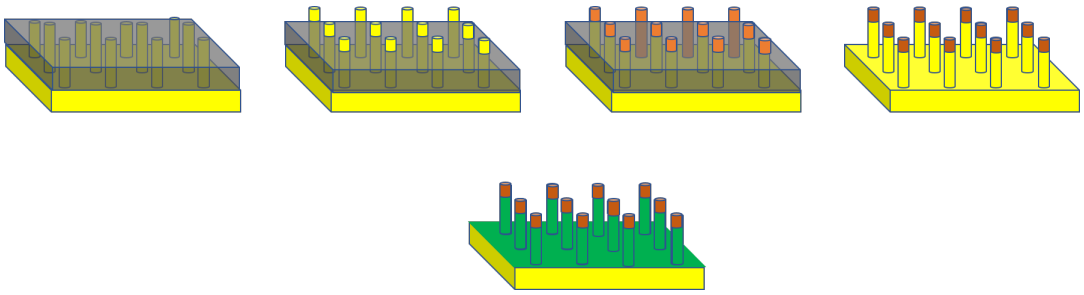

Figure 5.9: Purpose of the sacrificial layer in the bifunctionalization process. 1) PAA layer is spin-coated onto the surface. 2) Etching is performed to reveal and clean the top of the nanopillars. 3) First functionalization. 4) The PAA layer is removed revealing the remaining surface. 5) Second functionalization and resulting bifunctionalized sample

In order to obtain a PAA layer revealing only the top of the nanopillars after spin-coating and etching, different parameters need to be determined:

- the speed rotation for the spin-coating process (influencing thickness);
- the concentration of the PAA solution (influencing thickness);
- the etching power (influencing the amount of etched PAA);
- the etching process: RIE or chemical etching (influencing the amount of etched PAA).

However, a previous work related to this project already studied some of those parameters [93], allowing to use certain conclusions here:

- the rotational speed should be set to 1750 rpm/s because it was demonstrated to be the best compromise for obtaining layers with a good homogeneity without nanopillars bending or breaking;
- When using air plasma to perform the layer etching, contamination of the PAA layer by nitrogen was observed. Since this could possibly affect the dissolution of the PAA layer (step 4 in figure 5.9), RIE using oxygen is studied here to compare both etchings and eventually use oxygen RIE instead of air plasma.

Based on this, the following parameters are investigated here:

- two PAA concentrations of 50 and 75 mg/ml to observe the obtained thickness;
- try oxygen RIE and compare its efficiency with air plasma;

- different etching powers with oxygen RIE to see their influence on the amount of etched PAA.

Because gold samples are not compatible with ellipsometric measurements and there was a need to determine the conditions for PAA spin-coating and etching, silicon wafers were used. This allowed to first investigate on flat silicon wafers the evolution of the amount of etched PAA with increasing powers and determine to needed PAA concentration, the etching time and the etching power.
Afterwards, gold nanostructured samples could be covered with PAA based on the parameters found previously and AFM technique was used to investigate the PAA layer on gold samples before spin-coating, after spin-coating and after etching.

### 5.2.1 PAA spin-coating

Knowing the typical height of the nanopillars (350-400 nm), we targeted a PAA layer thickness around 300 nm. We therefore tried two concentrations (50 mg/ml and 75 mg/ml) based on the results obtained in the previous work [93].
Using a concentration of 50 mg/ml and 75 mg/ml, we obtained a thickness of 332 +- 2.3 nm and 400 +- 8 nm respectively. AFM was used complementarily to SEM to assess the covering of the gold nanopillars. Results are shown in figures 5.10, 5.11, 5.12 and 5.13 where the surface can be observed before spin-coating and after spin-coating both in 2D and 3D. There is a clear difference before and after spin-coating where we can see that pillars are immersed in PAA. The nanopillars seem to not break or bend based on those images. A general SEM picture (figure 5.14) was also taken of the spin-coated PAA layer and a cone-shaped coverage is clearly visible.

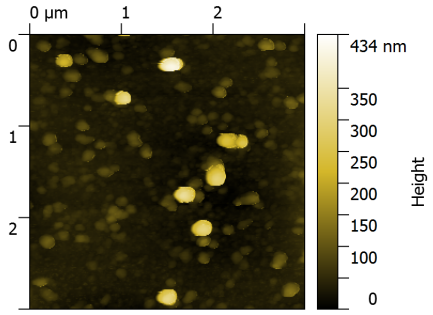


Figure 5.10: AFM image of the surface topography before spin-coating.

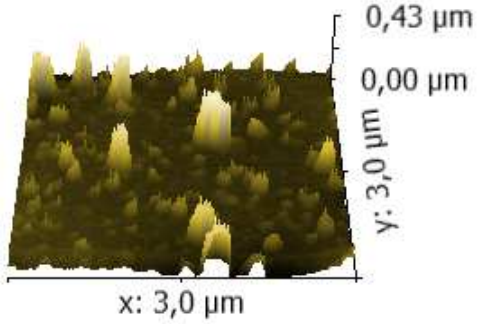


Figure 5.11: AFM 3D representation of the surface topography before spin-coating.

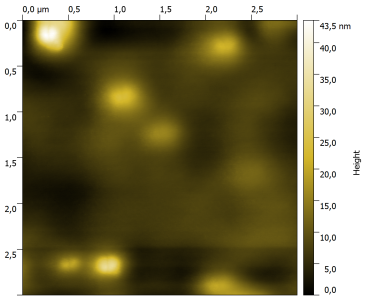


Figure 5.12: AFM image of the surface topography after spin-coating of a 50 mg/ml concentrated PAA solution.

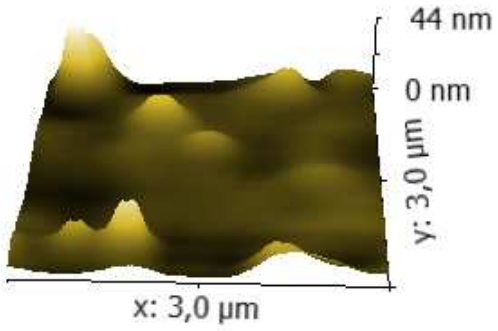


Figure 5.13: AFM 3D representation of the surface topography after spin-coating of a 50 mg/ml concentrated PAA solution.

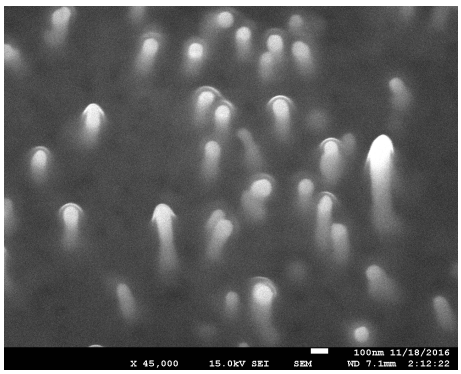


Figure 5.14: SEM image of the surface topography after spin-coating of a 50 mg/ml concentrated PAA solution

AFM 2D and 3D representations give a height difference of 44 nm between the top of the nanopillars and PAA layer which is a lower than what would theoretically be expect. However, this could be explained by the presence of the nanopillars on the surface that could alter the PAA deposition on the surface. Moreover, the fact that the nanopillars height do not follow a normal distribution could also be a possible reason for this difference since AFM measurements are performed on very localized spots and do therefore not reveal a general trend of the surface coverage.
As a conclusion, we can say that SEM and AFM images proved that nanopillars are not significantly affected by the PAA spin-coating (slight bending and no breaking seems to occur based on the SEM and AFM images) and the obtained film thickness can be used for further etching and bifunctionalization process.

### 5.2.2 PAA etching

As explained above, experiments using oxygen RIE have been conducted here to compare them to the results obtained in the previous work using air plasma [93].
To compare our calibrations curves obtained with ellipsometric measurements, the same PAA concentration of 75 mg/ml was used. Three etching powers were investigated here: 1, 2 and 3 W. This is because RIE combines two types of etching (chemical and physical) and is therefore more efficient at lower powers. Results of the calibration curves for the air plasma and oxygen RIE are given in figures 5.15 and 5.16. For oxygen RIE, we can observe that non-linear etching occurs at 3 W which is not the case at 1 and 2 W. Moreover, after 5 min, around 50 nm of PAA is etched

with powers of 2 and 3 W against 30 nm at 1 W.
For the AFM data comparison, experiments were performed in this work on both air plasma and oxygen RIE. For air plasma, etching was performed at 100 W for 2 min against 2 W for 10 min in oxygen RIE. 3D profiles after etching using oxygen RIE and air plasma are given in figure 5.17 and 5.18 respectively. PAA profile on the nanopillars after spin-coating and after etching are also given in figures 5.19 and 5.20.

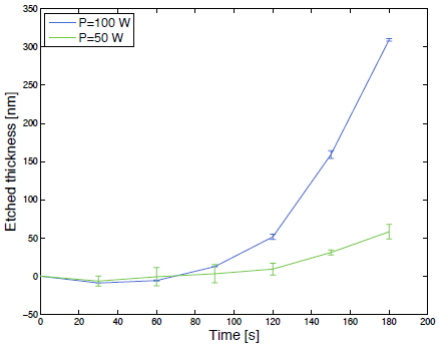


Figure 5.15: Calibration curve for air plasma treatment with a spin-coated PAA solution of concentration 75 mg/ml [93].

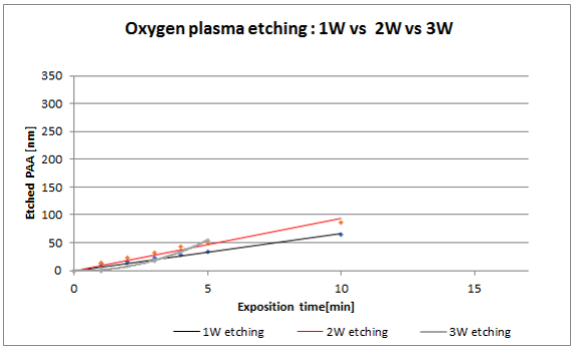


Figure 5.16: Calibration curve for oxygen RIE treatment with a spin-coated PAA solution of concentration 75 mg/ml.

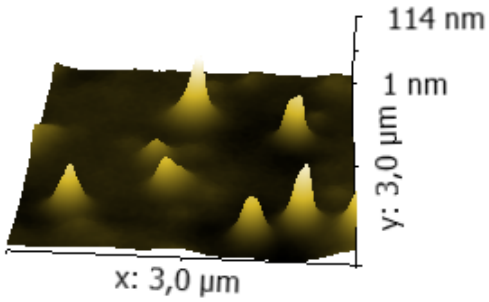


Figure 5.17: AFM 3D representation of the surface topography after oxygen RIE etching of the PAA layer spin-coated with a 50 mg/ml concentrated PAA solution.

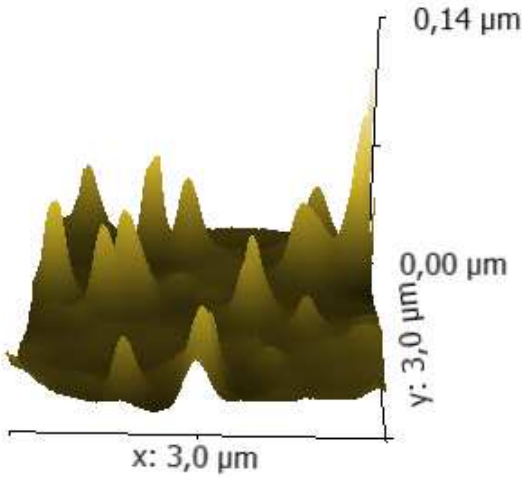


Figure 5.18: AFM 3D representation of the surface topography after air plasma etching of the PAA layer spin-coated with a 50 mg/ml concentrated PAA solution.

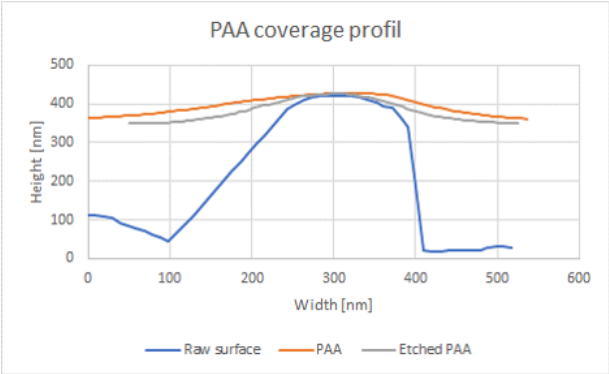


Figure 5.19: Typical PAA coverage profile of a nanopillar after spin-coating with a 50 mg/ml concentrated PAA solution and after etching using oxygen RIE.

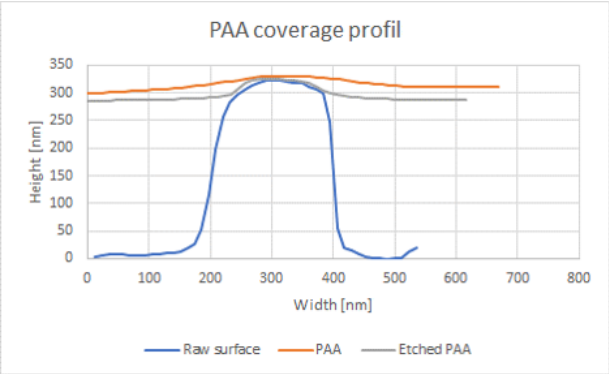


Figure 5.20: Typical PAA coverage profile of a nanopillar after spin-coating with a 50 mg/ml concentrated PAA solution and after etching using air plasma

When comparing results with the previous master thesis, we can see that etching is by far more effective with air plasma. This is observed on the calibration curves extracted from the PAA etching on silicon wafers as well as on the AFM images and PAA profiles extracted from nanostructured gold samples. Such differences could be explained by the powers and gas used for both process. Indeed, the powers used in oxygen RIE are much lower then the one used in air plasma. This yields to decreased ionization of oxygen and therefore decreased chemical and physical etching. The fact that RIE combines both etchings does not seem to overcome the chemical etching occurring with air plasma. Moreover, the reactive species created with oxygen gas could be less effective than the one created in air yielding to a better chemical etching in the case of air plasma.
If we use air plasma etching on a spin-coated PAA-layer which concentration is 50 mg/ml, this would yield theoretically to 100 nm of the top of the nanopillars that should be uncovered (44 nm before etching + 55 nm etched). This is confirmed by the AFM data where we can observe that most nanopillars pop around 100 nm. Therefore, we chose to use air plasma for the PAA layer etching despite the supposed contamination by nitrogen.

## 5.3 Functionalization on flat samples: Platinum vs Gold

Before working on nanostructured samples of platinum and gold, there was a need to observe the copolymer anchoring on flat surfaces as well as the grafting/release mechanism of PEG-SH used as model component. This section will thus study copolymer grafting and redox responsiveness on flat platinum and gold samples. The reason platinum was tested is because this metal is easier to electrodeposite and shows better mechanical properties when compared to gold. Therefore, higher aspect ratios could be reached without observing breaking or bending of the nanopillars which could be interesting in some applications such as cell culture. Figure 5.21 gives a schematic view of the conducted experiments.

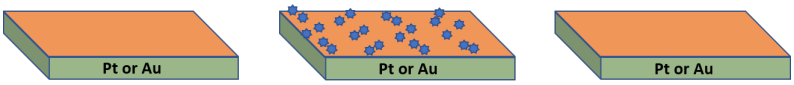


Figure 5.21: Schematic view of copolymer covering a platinum or gold surface followed by the anchoring/release process of PEG-SH on the copolymer.

### 5.3.1 Copolymer grafting

For this first experiment, two flat surfaces of gold an platinum where covered with the copolymer. The coverage of the surface was measured using CV. The results are given in figure 5.22 and 5.23, representing respectively the gold and platinum samples. The BF for those curves are respectively 96% and 18% meaning platinum samples are far less covered than gold samples.

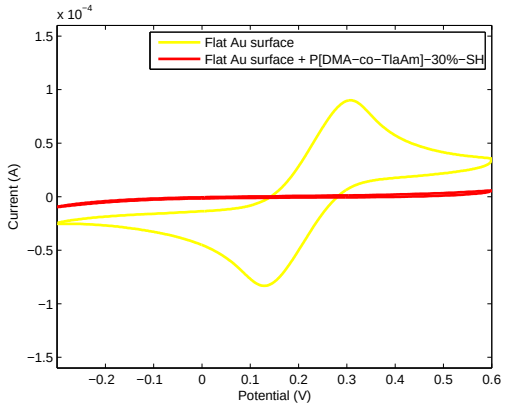


Figure 5.22: Copolymer grafted on the gold flat surface

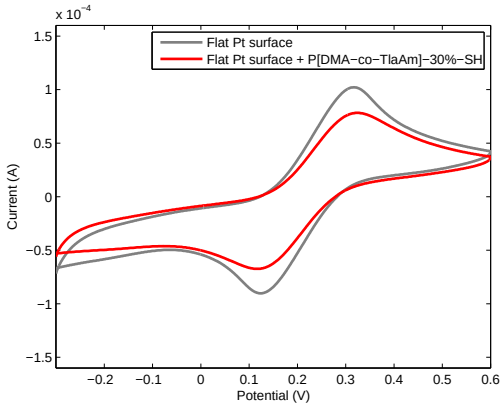


Figure 5.23: Copolymer grafted on the platinum flat surface

Prior to the copolymer grafting, the redox reactions occurring at the sample surface are limited by diffusion, explaining why diffusion peaks are observed on the voltammogram. After copolymer grafting, the curve is flattened because the copolymer layer acts as a insulator. No current should be observed if the surface was totally covered. However, the copolymer anchoring is not perfect explaining why a current are still observed. A comparison between both figures demonstrates that a poor anchoring occurred on the platinum sample compared to the gold sample. This is confirmed by the blocking factors obtained which show clear differences of surface coverage. An explanation could be the formation of an oxidized layer on the Pt surface which affects the copolymer anchoring (see section 3.3.1).

### 5.3.2 Copolymer redox responsiveness

Despite the fact the copolymer did not properly anchor and did not fully cover the Pt surface, PEG-SH anchoring and release process were tried on the platinum sample as well as on the gold sample. The schematic view of the designs is given in figure 5.24.

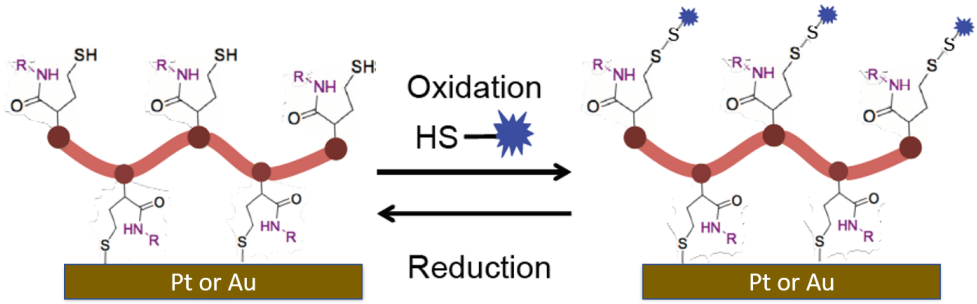


Figure 5.24: Experiment 1: Schematic view of the gold and platinum flat surfaces covered with P(DMA-co-TlaAm)-30% and with the redox process of anchoring and release of PEG-SH

EIS measurements were used to assess the anchoring and release and the results are shown in figure 5.25 and 5.26. Curve 1 represent the surface before PEG-SH grafting, curve 2 after PEG-SH grafting and curve 3 after PEG-SH release. Impedance values were also extracted from EIS measurements and are given on table 5.1.
We can observe that, in the case of gold, the anchoring and release of PEG-SH yields to increased and decreased resistance to charge transfer respectively. In the case of platinum, all three measures showed the presence of a diffusion limited redox process (straight line). Moreover, $R_{ct}$ was both increased when the platinum sample was exposed to PEG-SH in an oxidizing environment and a reducing environment with DTT.

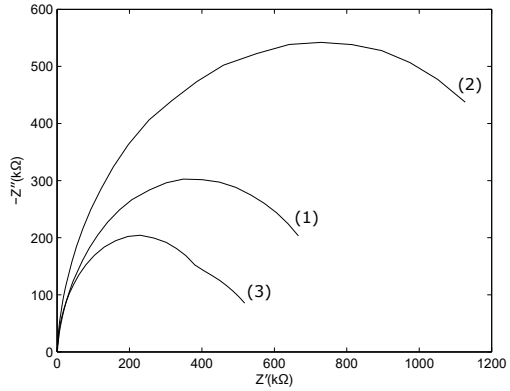


Figure 5.25: EIS measurements on a flat gold surface in three specific cases: 1. The surface is only covered by the copolymer (1) 2. Exposition to PEG-SH in an oxidative environment (2) 3. Exposition to a reductive environment (3)

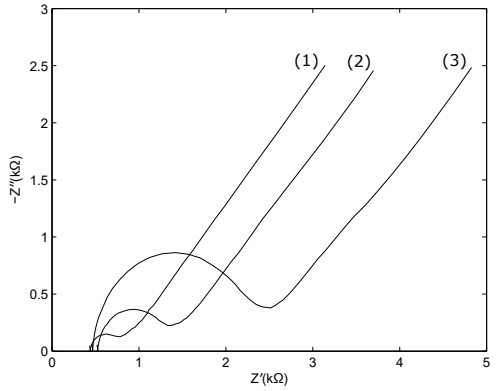


Figure 5.26: EIS measurements on a flat platinum surface in three specific cases: 1. The surface is only covered by the copolymer (1) 2. Exposition to PEG-SH in an oxidative environment (2) 3. Exposition to a reductive environment (3)

| | Copolymer only | Grafted PEG-SH | Released PEG-SH |
|---|---|---|---|
| Gold | 666 | 1127 | 518 |
| Platinum | 3.14 | 3.6 | 4.83 |

Table 5.1: Values of charge transfer resistances ($R_{ct}[k\Omega]$ for gold and platinum

For platinum samples, the presence of a diffusion-limited process is observed. This was expected since a poor surface coverage by the copolymer was observed earlier. This means that diffusion limited redox reactions occurs and yield to the straight line (see section 4.3.1). Concerning the evolution of $R_{ct}$ when exposed to PEG-SH, an increase is expected since PEG-SH will graft on the copolymer and eventually on the uncovered surface. When the sample is exposed to a reducing environment to release PEG-SH from the copolymer, $R_{ct}$ is supposed to decrease. However, an increase in $R_{ct}$ is observed, as if DTT reacts with the sample and the thiols from the DTT graft on the surface, increasing the resistance to charge transfer. Again, this is associated to the poor surface anchoring by the copolymer leaving large surfaces available for reactions between thiols and the uncovered surface. Based on those pore results on platinum, it was decided to continue the work with gold.

For the gold sample, that is nearly totally covered by the copolymer, results clearly show a good anchoring of PEG-SH, resulting in an increase of $R_{ct}$ observed through the EIS measurements. However, when the sample is exposed to a reductive environment, curve 3 is below curve 1 while they should have been equal (if all the PEG-SH had been released) which means that

PEG-SH was not the only released component from the sample and that copolymer was also partly detached.

## 5.4 Functionalization of gold nanopillars

This last section will provide the results obtained for nanostructured samples. First, cyclic voltammetry measurements obtained on a flat and bare nanostructured gold sample are compared. Afterwards, using again cyclic voltammetry, the bifunctionalization of nanostructured samples is studied. Finally, a method using silica nanoparticles for demonstrating the spatial bifunctionalization is proposed.
The characteristics of the nanostructured sample studied below are the following:

- Nanopillar density: $5 * 10^8\ cm^2$
- Height: 398 +- 43 nm
- Diameter: 81 +- 4 nm

### 5.4.1 Flat versus nanostructured samples

This sections aims to investigate the influence of nanopillars on electrochemical measurements before any functionalization. Measures were therefore performed on a bare flat gold sample and a bare nanostructured gold sample (figure 5.27).

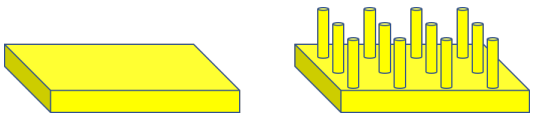

Figure 5.27: Schematic view of a bare flat gold sample (left) and bare nanostructured gold sample (right) used for the CV measurements

Results are shown in figure 5.28. Table 5.2 also gives an overview of the measured CV area in the case of a flat and nanostructured sample. We can observe that the measured current is slightly increased in the case of nanostructured samples compared to the flat sample while the shape are identical.

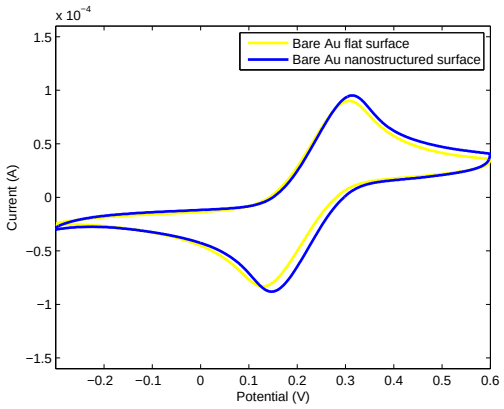


Figure 5.28: Comparison of flat bare surface and nanostructured bare surface

| | Flat sample | Nanostructured sample |
|---|---|---|
| CV area $[cm^2]$ | $1.7 * 10^{-5}$ | $2 * 10^{-5}$ |

Table 5.2: Comparison between flat and nanostructured surfaces

It can be observed that the peaks are at the same position but that in case of the nanostructured sample, the peak occurs higher, indicating higher currents are flowing through the surface. This can be explained by the increased sample surface due to the nanopillars, implying more surface available for redox reactions.

### 5.4.2 Copolymer and SAM grafting

This section exposes the results of the bifunctionalization process of a nanostructured gold surface. To this end, CV measurements were performed on three different samples as shown in figure 5.29: a bare nanostructured sample, a nanostructured sample where only the top of the nanopillars is covered by the copolymer and finally a bifunctionalized sample where the remaining surface (i.e. nanopillars base and bottom surface) is covered with the DDT layer. This allows to follow the evolution of the surface coverage when each functionalization is performed.

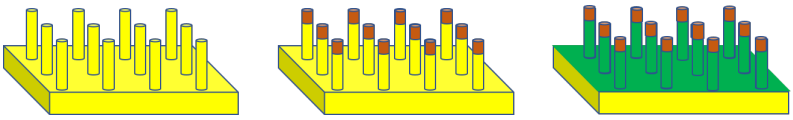

Figure 5.29: Schematic view of a bifunctionalized sample on which CV measurements were performed.

Results are shown in figure 5.30. Blocking factors after copolymer and SAM anchoring are also displayed in table 5.3. We can observe a a decrease in current flow occurring after respectively copolymer and SAM anchoring.

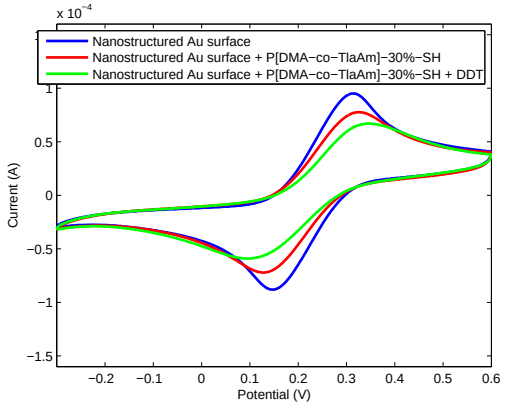


Figure 5.30: CV measurements of a nanostructured gold sample in three specific cases: 1. Bare nanostructured surface 2. Top of the nanopillars chemically modified with the copolymer 3. Bifunctionalized sample

| BF after copolymer grafting | BF after bifunctionalization |
|---|---|
| 12% | 24% |

Table 5.3: Blocking factor after the copolymer grafting and when the surface has been bifunctionalized

The voltammogram shows decreasing areas when the sample is submitted to the two successive functionalizations. The copolymer grafting gives expected results with a BF around 12%. Indeed, this could mean that the top of the nanopillars has been covered by the copolymer. However, the SAM grafting is far lower then expected since the BF factor should be around 100%. Indeed, even if current is decreased indicating the surface was covered by the SAM, the expected curve should not present this peak and should be more flattened like the one obtained in figure 5.22. This is because the copolymer and the SAM should act as a blocking layer the flow of an electric current. The reason explaining this difference could be the bad PAA layer dissolution in water. Indeed, presence of PAA could affect the DDT bonding on the surface.

### 5.4.3 Nanoparticles to assess spatial functionalization

As a last experiment, nanoparticles were used to assess the spatial bifunctionalization of the surface. Indeed, by using ethylenediamine instead of ethanolamine when unprotecting the polythiolactone copolymer, a positive charge is added to the copolymer that could consecutively interact with the negative charged silica nanoparticles. This was tried on nanostructured samples that were completely covered with the polythiolactone or the SAM. The purpose is to use this technique to obtain SEM images that show a bifunctionalized surface where silica nanoparticles would only adhere to the nanowire top, covered with the copolymer. Figure 5.31 details the strategy used for this technique.

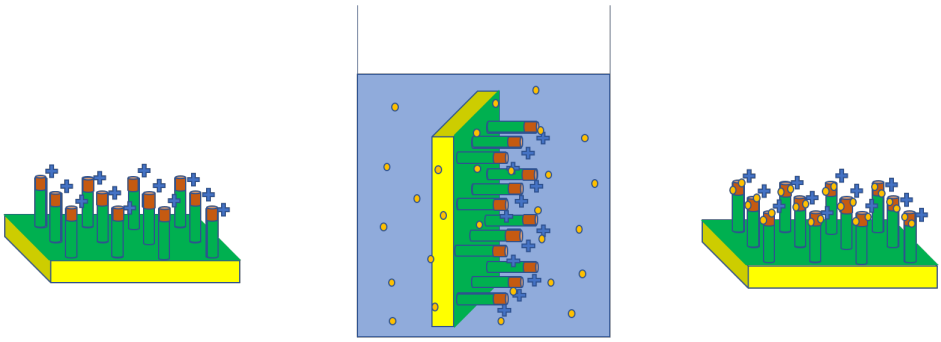

Figure 5.31: Schematic view of the adhesion of silica nanoparticles to the positively charged copolymer

Figures 5.32 and 5.33 shows the results obtained for surfaces covered respectively with the SAM and the charged copolymer.

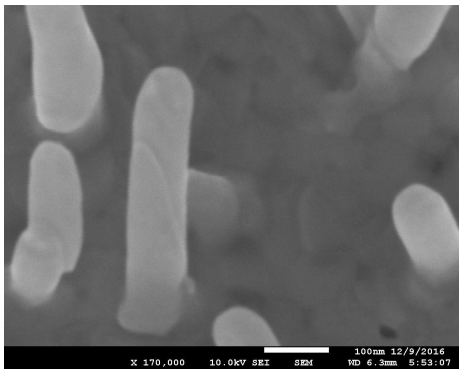


Figure 5.32: SEM image of a nanostructured surface covered with the DDT SAM and exposed to a solution containing silica nanoparticles

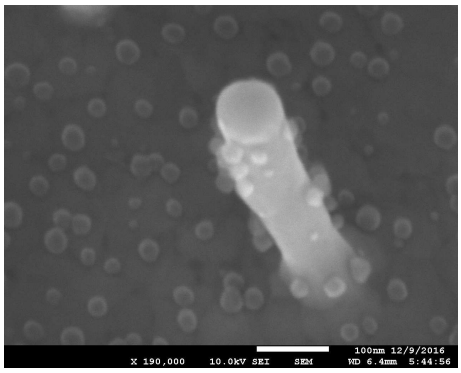


Figure 5.33: SEM image of a nanostructured surface covered with the charged copolymer and exposed to a solution containing silica nanoparticles

This technique seems promising since samples covered with DDT clearly show no sign of particle adhesion while the charged copolymer is obviously covered with nanoparticles thanks to the electrostatic interactions between the negatively charged silica nanoparticles and the positively charged copolymer. However, this technique needs to be further investigated on bifunctionalized samples.

# Chapter 6

# Conclusion

This work investigated a drug delivery strategy using nanostructured and stimuli responsive surfaces. First step was the nanostructuration process where a hard-templating approach was followed to elaborate nanopillars at the sample surface. Afterwards, the goal was to evaluate and assess a strategy that would allow the creation of bifunctionalized surfaces: the top of the nanopillars would be coated with a copolymer dedicated to the drug delivery process while the base of the nanopillars and the bottom surface would promote cell adhesion and nanopillars penetration into the cell cytosol.

The top of the nanopillars is functionalized with a polythiolactone copolymer in order to protect thiol functions from oxidation. The thiols are subsequently unprotected through aminolysis and some of them are involved in the surface anchoring while the others one are used for the anchoring of a model component, namely PEG-SH.
The PEG-SH grafting on the copolymer is performed through disulfide bonds in an oxidative environment (using CaT). The drug release is consecutively studied in a reductive environment (using DTT), as if it is exposed to the reductive medium of the cell.
In order to obtain bifunctionalized samples, functionalization of the top of the nanopillars is performed in presence of a sacrificial layer (PAA). Indeed, this layer covers temporarily the base of the nanopillars and the bottom surface and is afterwards removed to allow further functionalization of the remaining surface and obtain finally bifunctionalized surfaces.
This second functionalization is performed using a SAM of DDT.

The spin-coating of the sacrificial layer was studied to improve the results acquired in the previous master thesis [93]. Two PAA concentrations were investigated and conclusions lead to choose a 50 mg/ml concentration to obtain a layer thickness around 330 nm. Etching process was then studied to define the etching type, gas type, power and duration of the PAA etching. Conclusions yield to the use of the air plasma for a duration of 120 s and at a power of 100 W.

Flat surfaces were then studied using CV techniques in order to assess the copolymer anchoring both on platinum and gold samples. Conclusions lead to eliminate platinum as substrate because of the poor copolymer grafting onto the surface. Gold was therefore the only substrate studied afterwards when experiments were conducted on nanostructured samples.

The grafting/release process of the drug was then studied on flat surfaces using EIS measurements and redox responsiveness of the copolymer layer was assessed. However, it seemed that surface coverage was less important after drug release and this could possibly be due to partial copolymer detachment from the surface.

Bifunctionalization of samples was finally studied using CV measurements. It showed a limited coverage of the sample by DDT after PAA removal, possibly due to the bad PAA layer

dissolution.
A technique using silica nanoparticles was also proposed to show the spatial bifunctionalization and was tried on nanostructured samples fully functionalized with either DDT or positively charged copolymer. Good results were obtained (negatively charged silica particles adhered to the positively charged copolymer while no particles were observed on the DDT samples) but no images could be acquired afterwards showing the spatial bifunctionalization.

This work allowed to investigate the creation of bifunctionalized surfaces and proposed an innovative technique that would allow drug release and cell adhesion on a same surface. Further research should concentrate on understanding and improving the use of a sacrificial layer and the consecutive bifunctionalization process by understanding more deeply how it affects the surface and the consecutive functionalizations. Moreover, a technique showing spatial bifunctionalization should also be developed to confirm the selective grafting of the copolymer on the top of the nanopillars.

# Bibliography


[1] Park A and Wu. B. Griffith. Integration of surface modification and 3d fabrication techniques to prepare patterned poly(l-lactide) substrates allowing regionally selective cell adhesion. . *J Biomater Sci Polym*, 9, pp 89-110, 1998.

[2] P Banerjee, DJ Irivine, Mayes AM, and LG Griffith. : Polymer latexes for cell-resistant and cell-interactive surfaces. *J Biomed Mater Res*, 50, pp 331-339, 2000.

[3] Vande Vondele S andVoros J and Hubbell JA. Rgd-grafted poly-l-lysine-graft-(polyethylene glycol) copolymers block non-specific protein adsorption while promoting cell adhesion. *Biotechnol Bioeng*, 82: pp 784-790, 2003.

[4] Jort Robertus, Wesley R. Browne, , and Ben L. Feringa. Dynamic control over cell adhesive properties using molecular-based surface engineering strategies. *Chemical Society Reviews*, 39(1), pp 354-378, 2010.

[5] Robert L. Ehrmann and George O. Gey. The growth of cells on a transparent gel of reconstituted rat-tail collagen. *Journal of the National Cancer Institute*, 16(6), pp 1375-1403, 1956.

[6] John A. Ryan. Evolution of cell culture surfaces. *Biofiles*, 2008.

[7] Alberts B, Johnson A, and Lewis J et al. *Molecular Biology of the Cell*. New York: Garland Science, 4 edition, 2002.

[8] A.S.G. Curtis. The mechanism of adhesion of cells to glass. a study by interference reflection microscopy. *The Journal of Cell Biology*, 20(2), pp 199-215, 1964.

[9] Turner A. M. P., Dowell N., Turner S. W. P., Kam L., Isaacson M., Turner J. N., Craighead H. G., and Shain W. Attachment of astroglial cells to microfabricated pillar arrays of different geometries. *Journal of Biomedical Materials Research*, 51(3), pp 430-441, 2000.

[10] Turner A. M. P., Dowell N., Turner S. W. P., Kam L., Isaacson M., Turner J. N., Craighead H. G., and Shain W. Quantification of nanowire penetration into living cells. *Nat. Commun.*, 5, pp 3613-3621, 2014.

[11] Paula M Mendes. Stimuli-responsive surfaces for bio-applications. *Chem. Soc. Reviews*, 37(8), pp 2512-2529, 2008.

[12] Tokareva I., Minko S., Fendler J. H., and Hutter E. Nanosensors based on responsive polymer brushes and gold nanoparticle enhanced transmission surface plasmon resonance spectroscopy. *J. Am. Chem. Soc.*, 19, pp 3955–3961, 2009.

[13] Matttiasson B, Dainyak M.B, and Yu Galaev I. Smart polymers and protein purification. *Polymer-Plastic Technology and Engineering*, 37(3), pp 303-308, 1998.

[14] A. G. et al Skirtach. Laser-induced release of encapsulated materials inside living cells. *Angew. Chem. Int. Ed.*, 45, pp 4612–4617, 2006.

[15] Sabrina Belbekhouche, Stefan Reinicke, Pieter Espeel, Filip Du Prez, Pierre Eloy, Christine Dupont-Gillain, Alain Jonas, Sophie Demoustier, and Karine Glinel. Polythiolactone-based redox-responsive layers for the reversible release of functional molecules. *American Chemical Society*, 6,pp 22457-22466, 2014.

[16] W. Kim, J.Ng, M. Kunitake, B. Conklin, and P. Yang. Interfacing silicon nanowires with mammalian cells. *American Chemical Society*, 129, pp 7228-7229, 2007.

[17] Shalek et al. Vertical silicon nanowires as a universal platform for delivering biomolecules into living cells. *Proc. Natl Acad. Sci.*, 107, 1870-5, 2010.

[18] E. Ferain and R. Legras. Track-etch templates designed for micro- and nanofabrication. *Nuclear Instruments and Methods in Physics Research B*, 208, pp 115-122, 2003.

[19] P. Espeel and F. Du Prez. One-pot multi-step reactions based on thiolactone chemistry: A powerful synthetic tool in polymer science. *European Polymer Journal*, 62, pp 247-272, 2015.

[20] Guozhong Cao and Dawei Liu. Template-based synthesis of nanorod, nanowire, and nanotube arrays. *Advances in Colloid and Interface Science*, 136, pp 45-64, 2008.

[21] X. Duan and C. M. Lieber. General synthesis of compound semiconductor nanowires. *Advanced Materials*, 12(4), pp 298-302, 2000.

[22] Abhishek Chowdhurya and Avijit Misraa. Nanostructure growth using vls methods. *Advanced Materials*, 2010.

[23] R. C. Furneaux, W. R. Rigby, and A. P. Davidson. The formation of controlled-porosity membranes from anodically oxidized aluminium. *Nature*, 337, pp 147-149, 1989.

[24] A. Despic and VP. Parkhutik. *Modern Aspects of Electrochemistry.* Conway B.E., Et Al., 20 edition, 1989.

[25] D. AlMawlawi, N. Coombs, and M. Moskovits. Magnetic properties of fe deposited into anodic aluminum oxide pores as a function of particle size. *Journal of Applied Physics*, 70(8), pp 4421-4425, 1991.

[26] C.A. FossJr., M.J. Tierney, and C.R. Martin. Template synthesis of infrared-transparent metal microcylinders: comparison of optical properties with the predictions of effective medium theory. *Journal of Physical Chemistry*, 96(22), pp 9001-9007, 1992.

[27] P. Apel. Track etching technique in membrane technology. *Radiation Measurements*, 34, pp 559-566, 2001.

[28] Dr. Falk Münch. Ion track membranes and nano materials: Micro- and nanoporous polymer membranes, 2017.

[29] R. J. Tonucci, B. L. Justus, A. J. Campillo, and C. E. Ford. Nanochannel array glass. *Science*, 258(5083), pp 783-785, 1992.

[30] C. Wu and T. Bein. Conducting polyaniline filaments in a mesoporous channel host. *Science*, 264(5166), pp 1757-1759, 1994.

[31] S. Fan, M.G. Chapline, N. Franklin, T. Tombler, A. Cassell, and H. Dai. Self-oriented regular arrays of carbon nanotubes and their field emission properties. *Science*, 283(5401), pp 512-514, 1999.

[32] M. Knez, A. Bittner, F. Boes, C. Wege, H. Jeske, E. Mai, and K. Kern. Biotemplate synthesis of 3-nm nickel and cobalt nanowires. *Nano Letters*, 3(8), pp 1079-1082, 2003.

[33] R. Gasparac, P. Kohli, M. Mota, L.Trofin, and C.. Martin. Template synthesis of nano test tubes. *Nano Letters*, 4(3), pp 513-516, 2004.

[34] Y. Wang, K. Takahashi, H. Shang, and G. Cao. Synthesis and electrochemical properties of vanadium pentoxide nanotube arrays. *Journal of Physical Chemistry*, 109(8), pp 3085-3088, 2005.

[35] Marc Wirtz, Shufang Yu, and Charles R. Martin. Template synthesized gold nanotube membranes for chemical separations and sensing. *Analyst*, 127:pp 871-879, 2002.

[36] J B Mohler and H.J. Sedusky. *Electroplating for the metallurgist, engineer and chemist.* Chemical Pub. Co., 1 edition, 1951.

[37] T. M. Whitney, P. C. Searson, J. S. Jiang, and C. L. Chien. Fabrication and magnetic properties of arrays of metallic nanowires. *Science*, 261(5126), pp 1316-1319, 1993.

[38] C. Brumlik and C. Martin. Template synthesis of metal microtubules. *Journal of the American Chemical Society*, 113(8), pp 3174-3175, 1991.

[39] K.Singh, A. Martinez-Morales, K. Bozhilov, and M. Ozkan. A simple way of synthesizing single-crystalline semiconducting copper sulfide nanorods by using ultrasonication during template-assisted electrodeposition. *Chemistry of materials*, 19(10), pp 2446-2454, 2007.

[40] J. D. Klein, R. D. Herrick, D. Palmer, M. J. Sailor, C. Brumlik, and C. Martin. Electrochemical fabrication of cadmium chalcogenide microdiode arrays. *Chemistry of materials*, 5(7), pp 902-904, 1993.

[41] A. MacDiarmid. Nobel lecture: "synthetic metals": a novel role for organic polymers. *Review of Modern Physics*, 73(3), pp 701-712, 2001.

[42] K. Takahashi, S. Limmer, Y. Wang, and G. Cao. Growth and electrochemical properties of single-crystalline v2o5 nanorod arrays. *Japanese Journal of Applied Physics*, 44(1B), pp 662-668, 2005.

[43] Helen H. Lou and Yinlun Huang. Electroplating. *Encyclopedia of Chemical Processing*, pp 839–848, 2006.

[44] N. Kanani. *Electroplating: Basic Principles, Processes and Practice.* Elsevier Advanced Technology, 1 edition, 2004.

[45] Hui Li. Microfabrication techniques for producing freestanding multidimensional microstructures. *Microsystem Technology*, 22:pp 223-237, 2016.

[46] Marc Madoui. Fundamentals of microfabrication. *CRC Press LLC*, 1997.

[47] M.J. Madou. *Fundamentals of Microfabrication: The Science of Miniaturization.* CRC Press: Boca Raton, FL, USA, 2 edition, 2002.

[48] Vincent Linder et al. Water-soluble sacrificial layers for surface micromachining. *Small*, 7: pp 730-736, 2005.

[49] Martin Friz and Friedrich Waibel. Thin film deposition methods and characterization techniques. 2003.

[50] Dr. Ghanshyam Singh. Wet and dry etching. *Powerpoint Presentation (https://www.slideshare.net/gkdelhi8/slide-25-36278815)*, 2014.

[51] E. Meng. *Biomedical Microsystems*. CRC Press, 1 edition, 2010.

[52] P. Verdonck. Plasma etching.

[53] M. J. Madou. Fundamentals of microfabrication: The science of miniaturization. *Second edition*, 2002.

[54] Thierry : Plasma Science and Technology division. Dry etching (plasma etching) and wet etching and advantages and disadvantages of dry etching (plasma etching) and wet etching, 2017.

[55] Dr. Bruce K. Gale. Dry etching. Lecture done by Dr. Bruce K. Gale, Fundamentals of Micromachining, University of Utah.

[56] Avinash P. Nayak, Logeeswaran VY, and M. Saif Islam. Wet and dry etching.

[57] A. P. Alekhin, G. M. Boleiko, S. A. Gudkova, A. M. Markeev, A. A. Sigarev, V. F. Toknova, A. G. Kirilenko, R. V. Lapshin, E. N. Kozlov, and D. V. Tetyukhin. Synthesis of biocompatible surfaces by nanotechnology methods. *Nanotechnologies in Russia*, 5 (9–10), pp 696–708, 2010.

[58] Bertazzo S., Zambuzzi W. F., da Silva H. A., Ferreira C. V., and Bertran C. A. Bioactivation of alumina by surface modification: A possibility for improving the applicability of alumina in bone and oral repair. *Clinical Oral Implants Research*, 20, pp 288-293, 2009.

[59] Sara Morgenthaler, Seunghwan Lee, Stefan Zürcher, and Nicholas D. Spencer. A simple, reproducible approach to the preparation of surface-chemical gradients. *Langmuir*, 19, pp 10459-10462, 2003.

[60] S. Penttila, A. Toivonena, J. Lib, W. Zhengb, and R. Novotnyc. Effect of surface modification on the corrosion resistance of austenitic stainless steel 316l in supercritical water conditions. *The Journal of Supercritical Fluids*, 81, pp 157-163, 2013.

[61] David A. Rider, Ken D. Harris, Dong Wang, Jennifer Bruce, Michael D. Fleischauer, Ryan T. Tucker, Michael J. Brett, and Jillian M. Buriak. Thienylsilane-modified indium tin oxide as an anodic interface in polymer/fullerene solar cells. *ACS Applied Materials and Science*, 1, pp 279-288, 2008.

[62] Wataru Kubo, Masashi Nagao, Yoichi Otsuka, Tsutomu Homma, and Hirokatsu Miyata. Formation of multinuclear metal−terpyridyl complexes covalently bound to carbon substrates. *Langmuir*, 25, pp 13340-13343, 2009.

[63] M. Delamar, G. Désarmot, O. Fagebaume, R. Hitmi, J. Pinson, and J.-M. Savéant. Modification of carbon fiber surfaces by electrochemical reduction of aryl diazonium salts: Application to carbon epoxy composites. *Carbon*, 35(6), pp 801-807, 1997.

[64] X. J. Feng and L. Jiang. Design and creation of superwetting/antiwetting surfaces. *Advanced Materials*, 18(23), pp 3063-3078, 2006.

[65] T. P. Russell. Surface-responsive materials. *Science*, 297, pp 964-967, 2002.

[66] Bingwei Xin and Jingcheng Hao. Reversibly switchable wettability. *Chemical Society Reviews*, 39(2), pp 769-782, 2010.

[67] Huber Dale L, Manginell Ronald P., Samara Michael A., Kim Byung-Il, and Bunker Bruce C. Programmed adsorption and release of proteins in a microfluidic device. *Science*, 301, pp 352-354, 2003.

[68] Taolei Sun and Guangyan Qing. Biomimetic smart interface materials for biological applications. *Advanced Materials*, 23(12), pp H57-H77, 2011.

[69] Yong Qiu and Kinam Park. Environment-sensitive hydrogels for drug delivery. *Advanced Drug Delivery Reviews*, 64, pp 49-60, 2012.

[70] J. Christopher Love, Lara A. Estroff, Jennah K. Kriebel, Ralph G. Nuzzo, and George M. Whitesides. Self-assembled monolayers of thiolates on metals as a form of nanotechnology. *Chemical Reviews*, 105(4), pp 1103-1169, 2005.

[71] Jacob Israelachvili. *Intermolecular and Surface Forces*. Academic Press, 3 edition, 2011.

[72] Deepak Prashar. Self assembled monolayers -a review. *International Journal of ChemTech Research*, 4(1), pp 258-265, 2012.

[73] S. Jadhav. Self-assembled monolayers (sams) of carboxylic acids: an overview. *Central European Journal of Chemistry*, 9(3), pp 369-378, 2011.

[74] Quanmin Guo and Fangsen Li. Self-assembled alkanethiol monolayers on gold surfaces: Resolving the complex structure at the interface by stm. *Physical Chemistry Chemical Physics*, 16(36), pp 19074–19090, 2014.

[75] Abigail Pulsipher and Muhammad N. Yousaf. Self-assembled monolayers as dynamic model substrates for cell biology. *Advanced Polymer Science*, 240, pp 103-134, 2011.

[76] C. Canaria. Self-assembled monolayers for the study of biological targets. Master's thesis, California Institute of Technology, 5 2008.

[77] M. Mrksich, G. Sigal, and G. Whitesides. Self-assembled monolayers as dynamic model substrates for cell biology. *Langmuir*, 11(11), pp 4383-4385, 1995.

[78] K. Graf. Metal impurities in silicon device fabrication. *Springer-Verlag*, 1995.

[79] Shun-Chi Chang Zhiyong Li and R. Stanley Williams. Self-assembly of alkanethiol molecules onto platinum and platinum oxide surfaces. *Langmuir*, 19, pp 6744-6749, 2003.

[80] Jiang, Bruzewicz D. A., Thant M. M., and Whitesides G. M. Electrochemically deposited palladium as a substrate for self-assembled monolayers. *Langmuir*, 23(21), pp 10823-10830, 2007.

[81] Dong Gyu Jang, Soo Gyun Roh, Jong Hyo Kim, Wen Yi Jin, Jin Moo Seo, Myeong Ja Kwon, and Soo Min Lee. Synthesis of novel polythiol for plastic optical lens and its ophthalmic lens. *Bull. Korean Chem. Soc.*, 30(10), pp 2227-2232, 2009.

[82] Yan Chao Yuan, Min Zhi Rong, and Ming Qiu Zhang. Preparation and characterization of microencapsulated polythiol. *Polymer*, 49), pp 2531-2541, 2008.

[83] Renaud Nicolayl. Synthesis of well-defined polythiol copolymers by raft polymerization. *Macromolecules*, 45, pp 821-827, 2012.

[84] Harrison RG. The reaction of embryonic cells to solid structures. *J Exp Zool*, 17 , pp 521-544, 1914.

[85] Christopher J Bettinger, Robert Langer, and Jeffrey T Borenstein. Engineering substrate micro- and nanotopography to control cell function. *Angew Chem Int Ed Engl.*, 48(30) , pp 5406-5415, 2009.

[86] Laurent Bozec and Michael Horton. Topography and mechanical properties of single molecules of type i collagen using atomic force microscopy. *Biophys J.*, 88(6) , pp 4223-4231, 2005.

[87] Shan hui Hsu, Chun-Yu Chen, Po Seng Lu, Chao-Sung Lai, and Chun-Jung Chen. Oriented schwann cell growth on microgrooved surfaces. *Biotechnology and Bioengineering*, 92(5) , pp 579-588, 2005.

[88] M. Dalby, N. Gadegaard, R. Tare, A. Andar, M. Riehle, P. Herzyk, C. Wilkinson, and R. Oreffo. The control of human mesenchymal cell differentiation using nanoscale symmetry and disorder. *Nautre Materials*, 6(12)) , pp 997-1003, 2007.

[89] Christelle N Prinzl. Interactions between semiconductor nanowires and living cells. *Journal of Physics : Condensed Matter*, 27, 233103 (11p), 2015.

[90] Sara Bonde, Nina Buch-Manson, Katrine R Rostgaard, Tor Kristian Andersen, Trine Berthing, and Karen L Martinez. Exploring arrays of vertical one-dimensional nanostructures for cellular investigations. *Nanotechnology*, 25, 362001 (19pp), 2014.

[91] Bonde, T. Berthing, M.H. Madsen, T.K. Andersen, N. Buch-Manson, L. Guo, F. Li, X. Badique, K. Anselme, J. Nygard, , and K.L. Martinez. Tuning inas nanowire density for hek293 cell viability, adhesion, and morphology: Perspectives for nanowire-based biosensors. *ACS Applied Materials and Interfaces*, 5(21), pp 10510-10519, 2013.

[92] S.Y. Kim and E.G. Yang. Collective behaviors of mammalian cells on amine-coated silicon nanowires. *ACS Applied Materials and Interfaces*, 24(45), pp 455704, 2013.

[93] Annelies Bauwens. Nanostructured bioactive surfaces to control cell behaviour. Master's thesis, Université Catholique de Louvain, 6 2016.

[94] J. W. Finley, E. L. Wheeler, and S. C. Witt. Oxydation of gluthatione by hydrogen peroxide and other oxydizing agents. *American Chemical Society*, 29(2),pp 404-407, 1981.

[95] J. Wang. *Analytical Electrochemistry*. John Wiley & Sons, 2 edition, 2002.

[96] H. M. Jafari, L. Soleymnai, K. Abdelhalim, and R. Genov. Nanostructured cmos wireless ultra-wideband label-free pcr-free dna analysis soc. *IEEE Journal of Solid-State Circuits*, 49(5): pp 122-123, 2012.

[97] Claire Chattaway. Towards redox-responsive nanostructured surfaces for drug delivery application. Master's thesis, Université Catholique de Louvain, 6 2015.

[98] Gazala Ruhi and S.K. Dhawan. *Conducting Polymer Nano Composite Epoxy Coatings for Anticorrosive Applications, Modern Electrochemical Methods in Nano, Surface and Corrosion Science*. Dr. M. Aliofkhazraei, 2 edition, 2014.

[99] GAMRY Instruments. MS Windows NTbasics of electrochemical impedance spectroscopy, 2017.

[100] GAMRY Instruments. MS Windows NTbasics of electrochemical impedance spectroscopy, 2017.

[101] Harland G. Tompkins. MS Windows NT spectroscopic ellipsometry : What it is, what it will do and what it won't do, 2017.

[102] C. Schönenberger, B. M. I. van der Zande, L. G. J. Fokkink, M. Henny, C. Schmid, M. Krüger, A. Bachtold, R. Huber, H. Birk, and U. Staufer. Template synthesis of nanowires in porous polycarbonate membranes: electrochemistry and morphology. *American Chemical Society*, 101(28): pp 5497-5505, 1997.

[103] E. ferain and R. Legras. Characterisation of nanoporous particle track etched membrane. *Nucl. Instr. and Meth*, 131: pp 97-102, 1997.

Rue Archimède, 1 bte L6.11.01, 1348 Louvain-la-Neuve **www.uclouvain.be/epl**